Pentapartite Entanglement Measures of GHZ and W-Class State in the Noninertial Frame

Juan Luis Manríquez Zepeda [1] 📍, **Juvenal Rueda Paz** [1] 📍, **Manuel Avila Aoki** [1] **and Shi-Hai Dong** [2,3],*

[1] Centro Universitario UAEM Valle de Chalco, Universidad Autónoma del Estado de México, Ecatepec de Morelos 56615, Mexico; buzonjl@gmail.com (J.L.M.Z.); juvenal.rueda@gmail.com (J.R.P.); manvlk@hotmail.com (M.A.A.)

[2] Research Center for Quantum Physics, Huzhou University, Huzhou 313000, China

[3] Laboratorio de Información Cuántica, CIDETEC, Instituto Politécnico Nacional, UPALM, Mexico City 07700, Mexico

* Correspondence: dongsh2@yahoo.com

Abstract: We study both pentapartite GHZ and W-class states in the noninertial frame and explore their entanglement properties by carrying out the negativities including 1-4, 2-3, and 1-1 tangles, the whole entanglement measures such as algebraic and geometric averages π_5 and Π_5, and von Neumann entropy. We illustrate graphically the difference between the pentapartite GHZ and W-class states. We find that all 1-4, 2-3 tangles and the whole entanglements, which are observer dependent, degrade more quickly as the number of accelerated qubits increases. The entanglements of these quantities still exist even at the infinite acceleration limit. We also notice that all 1-1 tangles of pentapartite GHZ state $N_{\alpha\beta} = N_{\alpha_I\beta} = N_{\alpha_I\beta_I} = 0$ where $\alpha, \beta \in (A, B, C, D, E)$, whereas all 1-1 tangles of the W-class state $N_{\alpha\beta}$, $N_{\alpha_I\beta}$ and $N_{\alpha_I\beta_I}$ are unequal to zero, e.g., $N_{\alpha\beta} = 0.12111$ but $N_{\alpha_I\beta}$ and $N_{\alpha_I\beta_I}$ disappear at $r > 0.61548$ and $r > 0.38671$, respectively. We notice that the entanglement of the pentapartite GHZ and W-class quantum systems decays faster as the number of accelerated particles increases. Moreover, we also illustrate the difference of von Neumann entropy between them and find that the entropy in the pentapartite W-class state is greater than that of GHZ state. The von Neumann entropy in the pentapartite case is more unstable than those of tripartite and tetrapartite subsystems in the noninertial frame.

Keywords: GHZ and W-class states; negativity; von Neumann entropy; noninertial frame

PACS: 03. 67. a; 03. 67. Mn; 03. 65. Ud; 04. 70. Dy

1. Introduction

The transfer of quantum states between distant nodes of a quantum network is a basic task for quantum information processing. It is well known that all protocols used for quantum state transmission require entanglement between the sender and the receiver systems. Entanglement, which is at the basis of quantum mechanics and almost every quantum information protocol, has become a very interesting topic, particularly in many-body systems, with the recent development of quantum information technology. The correct understanding of entanglement is of importance due to its special application in many branches such as quantum teleportation, quantum communication and quantum cryptography [1–10], and quantum algorithms [11,12]. Moreover, it is also helpful in studying quantum communication protocols like quantum key distribution (QKD) [13].

Up to now, the development of quantum computing has required the study of multi-qubit entangled systems, so the entanglement properties of multipartite quantum systems under inertial frames are becoming more and more important. However, with the development of relativistic quantum information science, many authors have paid more and more

attention to the development of this field. In order to study the property of quantum entangled state existing in the noninertial frame, we have to employ a relativistic setting [14–16]. The relativistic quantum information regarded as a new interesting field has emerged for many years since the relation between quantum information science and relativity theory intermediated by quantum field theory allows us to have a deeper understanding of the fundamental principles in quantum mechanics [17,18]. This also helps us explore how the degree of entanglement would be affected in curved space time, particularly by the acceleration parameter. Until now, quantum information theory has been enriched by the contributions of quantum entanglement made in the noninertial frame [19–21]. The properties of multipartite entangled systems are mainly related to the acceleration parameter and the number of particles in the noninertial system, which undoubtedly affect the entanglement degree of the entangled system.

In recent years, many relevant and significant contributions to this field have been made [1,3,14–16,22–35]. For example, since several pure multipartite entangled systems was studied [25], where the Unruh effect was discussed [19–21], the entanglement has been verified as an observer dependent in the noninertial frame. Compared with the well-known entangled stated-GHZ state [15,36–41], the authors paid less attention to the W-class state because its density matrix cannot be written as an X matrix form. Nevertheless, we have employed a special technique to study the density matrix in the non-X matrix form and carried out the tripartite and tetrapartite W-class state cases [42–44], except for the generalized GHZ state in the noninertial frame [45–48]. After studying, we find that the degree of entanglement of the W-class state is more robust than the GHZ and generalized GHZ states. It should be recognized that the entanglement for tripartite and tetrapartite systems still exists even at the infinite acceleration limit. However, Ye and her collaborators carried out the enhancement of multipartite entanglement in an open system in the noninertial frame [49]. Other relevant studies such as the fidelity loss and coherence loss, etc., in the open systems have also been done in Refs. [8,10].

Generally speaking, two main entanglement measures, which are named as negativity and von Neumann entropy, have been used to quantify the genuine entanglement. The negativity is employed to study the multi-tangle and the whole entanglement measures. The von Neumann entropy is concerned with the stability of the entangled system. For example, the three tangle, i.e., 1-2 tangle [50], was proposed to study the entanglement property of the entangled quantum system when tripartite Alice, Bob, and Charlie initially shared an arbitrary fermionic three-qubit pure state as well as the later proposed π-tangle [36]. The three tangle has interesting properties, but its analytical calculation becomes a nontrivial task because its calculation depends on the negativities of bipartite and tripartite systems. Similarly, four tangle has been proposed when we studied the tetrapartite systems, which include 1-3 and 2-2 tangles [42,44,45,47,48]. Recently, stimulated by the study of the tripartite and tetrapartite W-class state [42–44], Sun and her coauthors studied the entanglement property of a pentapartite W-class state in the noninertial frame and showed how the acceleration parameter and the number of the accelerated qubits affect the entanglement property of the pentapartite W-class entangled system [51]. This was realized by studying the π-tangle, including the 1-4, 1-1 tangles and the von Neumann entropy. However, they were not concerned with the 2-3 tangle case due to its complication, which is also an important factor to describe the entanglement property of the entangled system. Moreover, as the W-class and GHZ states are the two most important pure states in quantum information, it is necessary to study their entanglement properties simultaneously and show their difference graphically. To enrich the paper [51], we shall present all 1-4, 2-3 tangles and von Neumann entropy for these two important pure states for completeness, which is the main purpose of this work.

This paper is organized as follows. In Section 2, we briefly review the transformation between Minkowski space and Rindler coordinates. How to construct the density matrix for the simplest case is presented. In Section 3, we study the negativities, including 1-4, 2-3, and 1-1 tangles, whole entanglement measures π_5 and Π_5 and von Neumann entropy, which

are illustrated graphically to show their difference. Finally, in Section 4 we summarize our conclusions.

2. Pentapartite Entanglement from One to Five Accelerated Observers

The pentapartite GHZ state that we are going to study in this work is given by

$$|\text{GHZ}\rangle = \frac{1}{\sqrt{2}}\Big(|0_A 0_B 0_C 0_D 0_E\rangle + |1_A 1_B 1_C 1_D 1_E\rangle\Big), \tag{1}$$

where $|0_A 0_B 0_C 0_D 0_E\rangle = |0_A\rangle \otimes |0_B\rangle \otimes |0_C\rangle \otimes |0_D\rangle \otimes |0_E\rangle$ so does the state $|1_A 1_B 1_C 1_D 1_E\rangle$, while the pentapartite W-class state has the following form [52]:

$$|\text{W}\rangle = \frac{1}{\sqrt{5}}\Big(|0_A 0_B 0_C 0_D 1_E\rangle + |0_A 0_B 0_C 1_D 0_E\rangle + |0_A 0_B 1_C 0_D 0_E\rangle + |0_A 1_B 0_C 0_D 0_E\rangle + |1_A 0_B 0_C 0_D 0_E\rangle\Big). \tag{2}$$

Here we use the subscripts A, B, C, D, and E to denote Alice, Bob, Charlie, David, and Elly (as we know, Eve is not of confidence), respectively. They initially share a pentapartite GHZ or W-class state in the inertial frame. In this work, we assume that the acceleration of particles always starts from the rightmost one in A(Alice), B(Bob), C(Charlie), D(David), E(Elly) qubits. That is to say, we first suppose that Elly is accelerated in a uniform acceleration but Alice, Bob, Charlie, and David remain stationary, and so on.

For entangled GHZ and W-Class states in the noninertial frame, let us use Rindler coordinates to describe a family of observers with a uniform acceleration and divide Minkowski space-time into two inaccessible regions I and II. The rightward accelerating observers are located in region I and causally disconnected from the analogous counterparts in region II [53,54]. Let us briefly review the connection between the vacuum and excitation states in Minkowski coordinates and those in Rindler coordinates. First, let Alice stay stationary, while Bob moves in a uniform acceleration. We consider Bob accelerated uniformly in the (t, z) plane. Rindler coordinates (τ, ζ) are appropriate for describing the viewpoint of an observer moving in a uniform acceleration. Two different sets of Rindler coordinates, which differ from each other by an overall change in sign, are necessary for covering Minkowski space. These sets of coordinates define two Rindler regions disconnected from each other, as shown in Figure 1 [16,55]:

$$\begin{aligned} t = a^{-1} e^{a\zeta} \sinh(a\tau), \ z = a^{-1} e^{a\,\zeta} \cosh(a\tau), \ \text{Region I}, \\ t = -a^{-1} e^{a\zeta} \sinh(a\tau), \ z = -a^{-1} e^{a\,\zeta} \cosh(a\tau), \ \text{Region II}. \end{aligned} \tag{3}$$
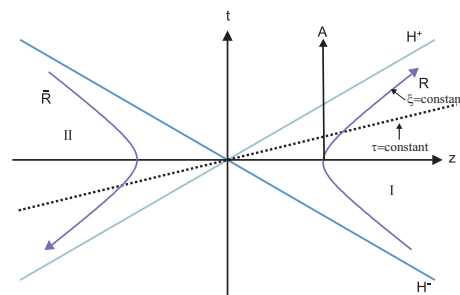

Figure 1. Rindler space time diagram: lines of constant position ζ are hyperbolas and lines of constant proper time τ for the accelerated observer run through the origin. In present work, we denote regions I and II as Bob and anti-Bob, respectively. The reader can refer to Ref. [55] for more information.

A free Dirac field in $(3+1)$ dimensional Minkowski space satisfies the Dirac equation $i\gamma^\mu \partial_\mu \psi - m\psi = 0$, where m is the particle mass and γ^μ the Dirac gamma matrices. A spinor wave function ψ composed of the complete orthogonal set of fermion ψ_k^+ and antifermion ψ_k^- modes can be expressed as $\psi = \int (a_k \psi_k^+ + b_k^\dagger \psi_k^-) dk$, where $a_k^\dagger (b_k^\dagger)$ and $a_k (b_k)$ are the creation and annihilation operators for fermions (antifermions) of the momentum k, respectively, satisfying the relation $\{a_i, a_j^\dagger\} = \{b_i, b_j^\dagger\} = \delta_{ij}$. The quantum field theory for a

Rindler observer is constructed by expanding the spinor field in light of a complete set of fermion and antifermion modes in regions I and II as follows:

$$\psi = \int \sum_\tau (c_k^\tau \psi_k^{\tau+} + d_k^{\tau\dagger} \psi_k^{\tau-}) dk, \quad \tau \in \{\mathrm{I, II}\}. \tag{4}$$

In a similar way, $c_k^{\tau\dagger}(d_k^{\tau\dagger})$ and $c_k^\tau(d_k^\tau)$ are the creation and annihilation operators for fermion (antifermions), respectively, acting on region I (II) for $\tau = \mathrm{I}$ (II) and also satisfy a similar anticommutation relation. The relation between creation and annihilation operators in Minkowski and Rindler space times can be found by the Bogoliubov transformation

$$a_k = \cos(r)\, c_k^{\mathrm{I}} - \sin(r)\, d_{-k}^{\mathrm{II}\dagger}, b_k = \cos(r)\, d_k^{\mathrm{I}} - \sin(r)\, c_{-k}^{\mathrm{II}\dagger}, \tag{5}$$

where $\cos(r) = 1/\sqrt{1 + e^{-2\pi\omega_k c/a}}$ with $\omega_k = \sqrt{|\mathbf{k}|^2 + \mathrm{m}^2}$ and r is a Bob's acceleration parameter with the range $r \in [0, \pi/4]$ for $a \in [0, \infty)$. It is known from this equation and its adjoint that Bogoliubov transformation mixes a fermion in region I and antifermions in region II. As a result, it is assumed that the Minkowski particle vacuum state for mode k based on Rindler Fock states is given by

$$|0_k\rangle_M = \sum_{n=0}^1 A_n |n_k\rangle_I^+ |n_{-k}\rangle_{II}^-, \tag{6}$$

where the Rindler region I or II Fock states carry a subscript I and II, respectively, on the kets, but the Minkowski Fock states are indicated by the subscript M on the kets. As what follows, we are only interested in using single mode approximation [15,16,24,56–59], i.e., $w_{A,B,C,D} = w$ and also uniform acceleration $a_{A,B,C,D} = a$ ($a_{w,M} \approx a_{w,U}$ is considered to relate Minkowski and Unruh modes) for simplicity.

Using the single mode approximation, one can transform Bob's vacuum state $|0_B\rangle_M$ and one-particle state $|1_B\rangle_M$ in Minkowski space into Rindler space. Using the creation and annihilation operators on Equation (6) above and using the normalization condition, we can obtain [15,16,24,56–59]

$$
\begin{aligned}
|0\rangle_M &= \cos(r)|0_I 0_{II}\rangle + \sin(r)|1_I 1_{II}\rangle, \\
|1\rangle_M &= |1_I 0_{II}\rangle,
\end{aligned}
\tag{7}
$$

where $|n_{B_I}\rangle$ and $|n_{B_{II}}\rangle$ ($n = 0, 1$) are the mode decomposition of $|n_B\rangle$ into two causally disconnected regions I and II in Rindler space. It should be pointed out that Bruschi et al. discussed the Unruh effect *beyond* the single mode approximation [21], in which two complex numbers q_R and q_L (the subindexes L and R corresponding to the Left and Right regions in Rindler diagram, i.e., regions I and II) are used to construct the one-particle state, i.e., $|1\rangle = q_R|1_R 0_L\rangle + q_L|0_R 1_L\rangle$. However, in the present case for single mode approximation, one has $q_R = 1, q_L = 0$ to satisfy the normalization condition $|q_R|^2 + |q_L|^2 = 1$. It is also worth noting that a Minkowski mode that defines the Minkowski vacuum is related to a highly nonmonochromatic Rindler mode rather than a single mode with the same frequency (see Refs. [21,30,60,61] for details). Other relevant contributions [31,59,62–65] have also been made.

To illustrate how to expand $|GHZ\rangle$ in Rindler coordinates, we are going to give explicit expression when Elly is accelerated, i.e.,

$$|GHZ\rangle_{ABCDE_I E_{II}} = \frac{1}{\sqrt{2}} \Big(\cos(r)|0_A 0_B 0_C 0_D 0_{E_I} 0_{E_{II}}\rangle + \sin(r)|0_A 0_B 0_C 0_D 1_{E_I} 1_{E_{II}}\rangle + |1_A 1_B 1_C 1_D 1_{E_I} 0_{E_{II}}\rangle \Big). \tag{8}$$

Similarly, we can also obtain the expressions of other cases when the observers Alice, Bob, Charlie, and David are accelerated. Such a procedure also works for the pentapartite W-class $|W\rangle$ case.

After the transformation to the Rindler space, we have to trace out the part of the antiparticle state in region II from the density matrix $\rho_{ABCDE_I} = \mathrm{Tr}_{E_{II}} |\mathrm{GHZ}\rangle_{ABCDE_I E_{II}} \langle \mathrm{GHZ}|$. In this case, when Elly is accelerated, the corresponding density matrix is thus given by

$$
\begin{aligned}
\rho_{ABCDE_I} = \frac{1}{2} \Big(& \cos^2(r) |0_A 0_B 0_C 0_D 0_{E_1}\rangle \langle 0_A 0_B 0_C 0_D 0_{E_I}| + \cos(r) |0_A 0_B 0_C 0_D 0_{E_I}\rangle \langle 1_A 1_B 1_C 1_D 1_{E_I}| \\
& + \cos^2(r) |0_A 0_B 0_C 0_D 1_{E_I}\rangle \langle 0_A 0_B 0_C 0_D 1_{E_I}| + \cos(r) |0_A 0_B 0_C 0_D 0_{E_I}\rangle \langle 1_A 1_B 1_C 1_D 1_{E_I}| \\
& + |1_A 1_B 1_C 1_D 1_{E_I}\rangle \langle 1_A 1_B 1_C 1_D 1_{E_I}| \Big).
\end{aligned}
\tag{9}
$$

For simplicity, we write out explicitly all nonzero elements $[i, j]$ for pentapartite GHZ and W-class states in Appendix A. These results will be helpful in calculating the negativity and von Neumann entropy, as shown below.

3. Entanglement Measures: Negativity and von Neumann Entropy

3.1. Negativity

Negativity, which is used to measure the entanglement of multipartite systems, is defined by [66–68]

$$
N_{\alpha, \beta\gamma\delta\epsilon} = ||\rho_{\alpha, \beta\gamma\delta\epsilon}^{T_\alpha}|| - 1, \quad N_{\alpha\beta, \gamma\delta\epsilon} = ||\rho_{\alpha\beta(\gamma\delta\epsilon)}^{T_{\alpha\beta}}|| - 1, \quad N_{\alpha, \beta} = ||\rho_{\alpha\beta}^{T_\alpha}|| - 1,
\tag{10}
$$

where $N_{\alpha, \beta\gamma\delta\epsilon}$, $N_{\alpha\beta, \gamma\delta\epsilon}$ and $N_{\alpha, \beta}$ represent 1-4, 2-3, and 1-1 tangles, respectively. The expressions $||\rho_{\alpha(\beta\gamma\delta\epsilon)}^{T_\alpha}||$, $||\rho_{\alpha\beta(\gamma\delta\epsilon)}^{T_{\alpha\beta}}||$ and $||\rho_{\alpha\beta}^{T_\alpha}||$ are the trace norms of the partial transposes of the density matrices. Generally speaking, the trace of any Hermitian operator A is equal to the sum of its eigenvalues [69], $||A|| = \mathrm{tr}\sqrt{A^\dagger A}$, i.e.,

$$
||M|| - 1 = 2 \sum_{i=1}^{N} |\lambda_M^{(-)}|^i,
\tag{11}
$$

where $\lambda_M^{(-)}$ represents the negative eigenvalue of the matrix M. It should be pointed out the calculation of these negativities is very complicated and time consuming.

Let us first calculate the negativity 1-4 tangle for the GHZ and W-class states when 1 to 5 observer(s) is (are) accelerated. The explicit expressions of the pentapartite GHZ and W-class states are written out in Appendix B for completeness. (It should be pointed out that the special symbols such as Root, #, and & appeared in this Appendix B and also in Appendix C are generated systematically by Wolfram Mathematica.) In Figure 2, we plot the negativity 1-4 tangle of pentapartite GHZ and W-class states when only one of five observers is accelerated. It is seen in Figure 2a that the $N_{A,BCDE_1} = N_{B,ACDE_1} = N_{C,ABDE_1} = N_{D,ABCE_1}$ decreases from 1 to $1/\sqrt{2}$ (29.29% loss of entanglement), whereas the $N_{E_1,ABCD}$ decreases from 1 to 0.5 (50% loss of entanglement). This means that entanglement is observer dependent. Furthermore, in the case of the W-class state as shown in Figure 2b, the $N_{A,BCDE_1}$ decreases from 0.8 to 0.7048 (11.891% loss of entanglement), but $N_{E_1,ABCD}$ decreases from 0.8 to 0.29282 (63.4% loss of entanglement).
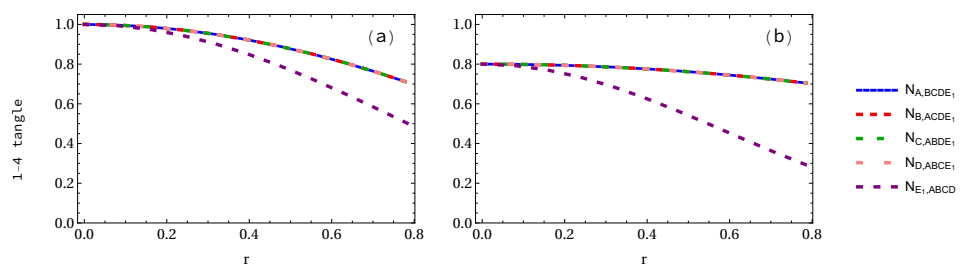

Figure 2. Panels (**a**,**b**) show the variation of 1-4 tangle with the parameter r in the case of pentapartite GHZ and W-class states, respectively, when only one qubit is accelerated.

In Figure 3, we plot the negativity 1-4 tangle when two observers are accelerated. As shown in Figure 3a, the negativity 1-4 tangle $N_{A,BCD_1E_1} = N_{B,ACD_1E_1} = N_{C,ABD_1E_1}$ in the pentapartite GHZ system decreases from 1 to 0.5 (50% loss of entanglement), whereas $N_{E_1,ABCD_1} = N_{D_1,ABCE_1}$ decreases to 0.3903 (60.97% loss of entanglement). In the case of the W-class state as displayed in Figure 3b, the negativity N_{A,BCD_1E_1} decreases from 0.8 to 0.5924 (25.94% loss of entanglement), whereas the $N_{E_1,ABCD}$ decreases from 0.8 to 0.24515 (81.86% loss of entanglement). We may conclude that the negativity N_{A,BCD_1E_1} in the GHZ state decays faster than that of W-class state, but $N_{E_1,ABCD_1}$ in the GHZ state decays slower than that of W-class state.
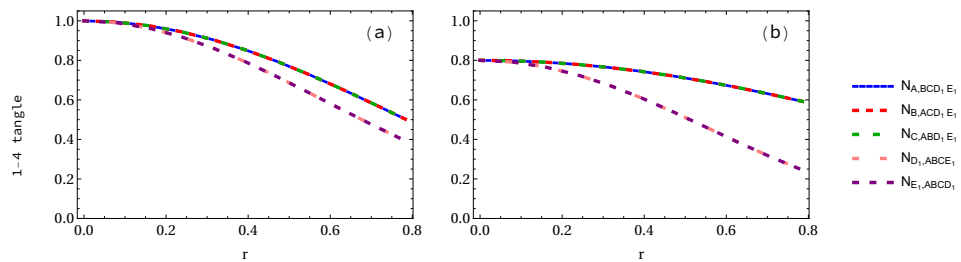

Figure 3. Same as Figure 2 but when two qubits are accelerated.

In Figure 4, we plot the negativity 1-4 tangle when three observers are accelerated. We can see in Figure 4a that negativity $N_{A,BC_1D_1E_1} = N_{B,AC_1D_1E_1}$ in the GHZ pentapartite system decreases from 1 to $1/2\sqrt{2}$ (64.65% loss of entanglement), and $N_{E_1,ABC_1D_1} = N_{C_1,ABD_1E_1} = N_{D_1,ABC_1E_1}$ decreases to 0.2965 (70.35% loss of entanglement). However, in the case of the W-class state as shown in Figure 4b, $N_{A,BC_1D_1E_1}$ decreases from 0.8 to 0.4529 (43.38% loss of entanglement), whereas N_{E_1,ABC_1D_1} decreases to 0.1966 (75.41% loss of entanglement).
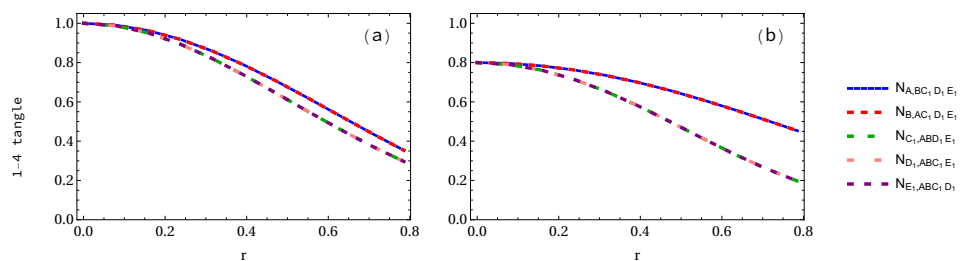

Figure 4. Same as Figures 2 and 3 but when three qubits are accelerated.

In Figure 5, we plot the negativity 1-4 tangle when four observers are accelerated. We can see in Figure 5a that negativity $N_{A,B_1C_1D_1E_1}$ in the GHZ pentapartite state decreases from 1 to 0.2206 (77.94% loss of entanglement), and $N_{E_1,AB_1C_1D_1} = N_{D_1,AB_1C_1E_1} = N_{C_1,AB_1D_1E_1} = N_{B_1,AC_1D_1E_1}$ decreases also from 1 to 0.2206 (77.94% loss of entanglement). It should be emphasized that the negativities $N_{A,B_1C_1D_1E_1}$ and $N_{E_1,AB_1C_1D_1}$ at both $r = 0$ and $r = \pi/4$ are the same, but their explicit expressions given in Appendix B are not the same. Moreover, for the W-class state as shown in Figure 5b, the $N_{A,B_1C_1D_1E_1}$ decreases from 0.8 to 0.1870 (76.62% loss of entanglement), but $N_{E_1,AB_1C_1D_1}$ decreases to a smaller value 0.1436 (82.04% loss of entanglement). We find that the difference of the loss of entanglement for both $N_{E_1,AB_1C_1D_1}$ and $N_{A,B_1C_1D_1E_1}$ of two different pentapartite states is very small.

Finally, we find that negativity $N_{A_1,B_1C_1D_1E_1}$ in the case of GHZ state decreases from 1 to 0.1455 (85.45% loss of entanglement) as seen in Figure 6a, whereas $N_{A,B_1C_1D_1E_1}$ as shown in Figure 6b in the W-class state decreases from 0.8 to 0.0596 (92.54% loss of entanglement). This means that the entanglement of these two pentapartite quantum systems decay most when all particles are accelerated.
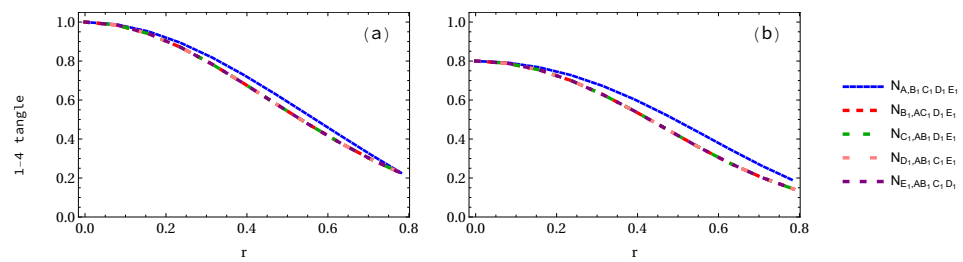
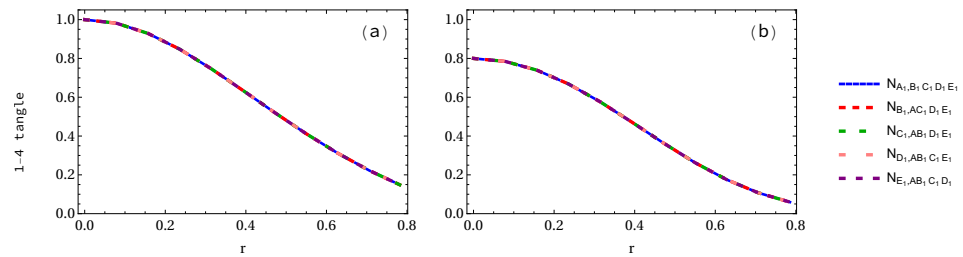**Figure 5.** Same as above but when four qubits are accelerated.

Figure 6. Same as above but when all qubits are accelerated.

In Figures 7a,b and 8a,b, we show how the entanglement changes with the number of the accelerated qubits if we only refer to Alice and Elly. It is found that the negativity decreases as the number of accelerated qubits increases, but negativity in the W-class state decreases faster than that in the GHZ state when Elly is taken as a reference (see Figure 8).
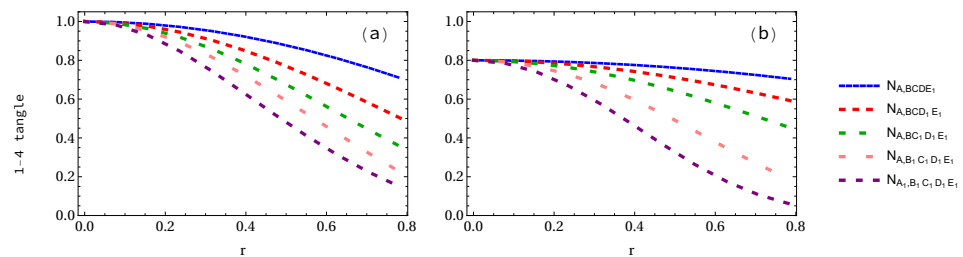

Figure 7. Panels (**a**,**b**) corresponding to GHZ and W-class states with respect to Alice show the variations of the 1-4 tangle for 1 to 5 arbitrary selected qubits as a function of the acceleration parameter r.
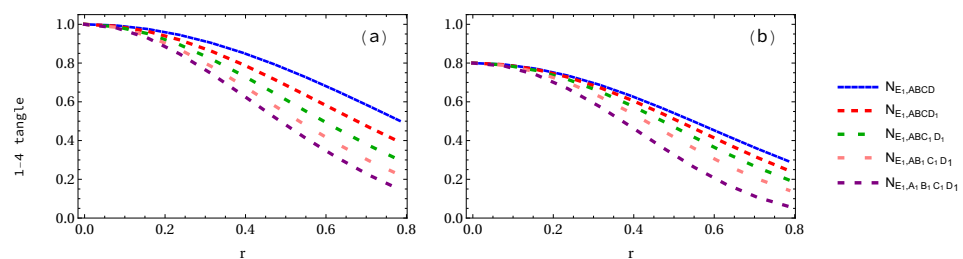

Figure 8. Same as Figure 7 but with respect to Elly.

To calculate the whole entanglement measures such as algebraic and geometric averages π_5 and Π_5, we have to find the 1-1 tangle of both GHZ and W-class states. In the case of the GHZ state, all 1-1 tangles are equal to zero. In the case of the W-class state, however, some of them that are unequal to zero are expressed as

$$N_{\alpha,\beta} = \frac{1}{5}(\sqrt{13}-3) = 0.12111,$$

$$N_{\alpha_I,\beta} = \frac{1}{5}(\sqrt{5+6\cos 2r + 2\cos 4r} - \cos 2r - 2), \qquad (12)$$

$$N_{\alpha_I,\beta_I} = \frac{1}{20}(4\cos 2r - 3\cos 4r - 13 + 2\sqrt{2}\sqrt{21 - 12\cos 2r + 17\cos 4r}),$$

where $\alpha, \beta \in (A, B, C, D, E)$ and $N_{\alpha,\beta} > N_{\alpha_I,\beta} > N_{\alpha_I,\beta_I} > N_{\alpha,\beta_1} = 0$. The $N_{\alpha,\beta}$, $N_{\alpha_I,\beta}$, and N_{α_I,β_I} represent the bipartite subsystems with 0 to 2 accelerated qubits. As shown in Figure 9, it is interesting to see that the entanglement in the 1-1 tangle $N_{\alpha_I,\beta}$ vanishes at $r > 0.61548$ (only one accelerated particle), but N_{α_I,β_I} vanishes at $r > 0.38671$ (two accelerated particles), except for a constant $N_{\alpha,\beta} = 0.12111$.
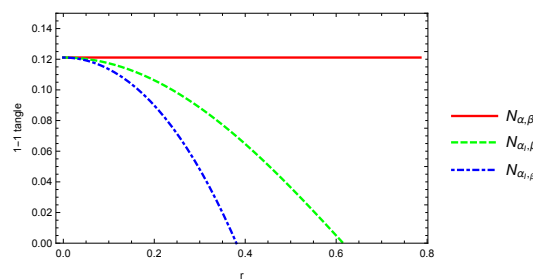

Figure 9. Plot of 1-1 tangle for pentapartite W-class state as a function of acceleration parameter r.

We are now in the position to study negativity 2-3 tangle even though it is not required to calculate the whole entanglement measures. However, we want to present them for completeness, as these results have never been presented to our best knowledge. The analytical expressions of both GHZ and W-class states are given in Appendix C. It is found that the negativity of GHZ state at $r = 0$ is 1, whereas in W-class state it is 0.979796. As the acceleration parameter r increases, they all decrease with it, but in W-class state decreases faster than that in the GHZ state. Negativity 2-3 tangle is also dependent on the number of accelerated observers. When only one qubit is accelerated in the GHZ pentapartite state, as displayed in Figure 10a, we notice that $N_{AB,CDE_1} = N_{AE_1,BCD}$ are equal to each other, but N_{AB,CDE_1} and $N_{AE_1,BCD}$ are not the same, as shown in Figure 10b. At the infinite acceleration limit, the 2-3 tangle for GHZ state decreases from 1 to $1/\sqrt{2}$ (29.3% loss of entanglement) at $r = \pi/4$, but 2-3 tangle N_{AB,CDE_1} and $N_{DE_1,ABC}$ in the case of W-class state, as shown in Figure 10b, decrease from 0.979796 to 0.8195 (16.35% loss of entanglement) and 0.7278 (25.71% loss of entanglement), respectively.
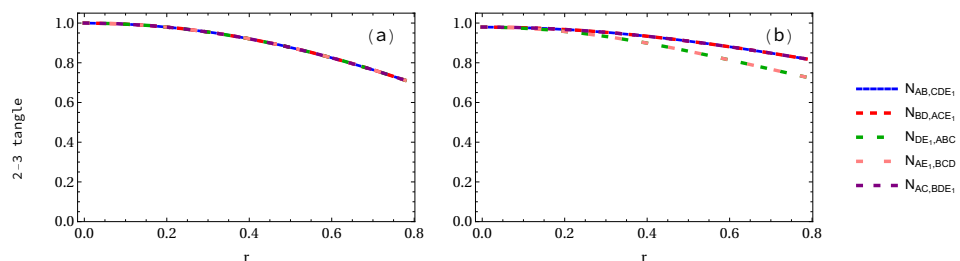

Figure 10. Panels (**a**,**b**) show the 2-3 tangle for both GHZ and W-class states, respectively, when one qubit is accelerated.

When two accelerated observers are considered (see Figure 11), it is found that $N_{D_1E_1,ABC}$ decreases faster than that of $N_{AB,CD_1E_1} = N_{AE_1,BCD_1}$ in the case of GHZ state. In the W-class case, the difference between $N_{AB,CD_1E_1} = N_{AC,BD_1E_1}$ and $N_{AE_1,BCD_1} = N_{BD_1,ACE_1}$ is almost equal to zero, but the difference between $N_{D_1E_1,ABC}$ and others such as N_{AE_1,BCD_1}

and N_{AB,CD_1E_1} is very big. At the infinite acceleration limit, in the case of GHZ state the 2-3 tangles $N_{AB,CD_1E_1} = N_{BD_1,ACE_1}$ and $N_{D_1E_1,ABC}$ are equal to 0.5 and 0.3903, respectively, but N_{AB,CD_1E_1} and $N_{D_1E_1,ABC}$ in the case of W-class state are equal to 0.6159 and 0.2274, respectively. This implies that the negativity N_{AB,CD_1E_1} in the W-class state is bigger than that of GHZ state, whereas $N_{D_1E_1,ABC}$ in the W-class state is smaller than that of GHZ state in the infinite acceleration limit.
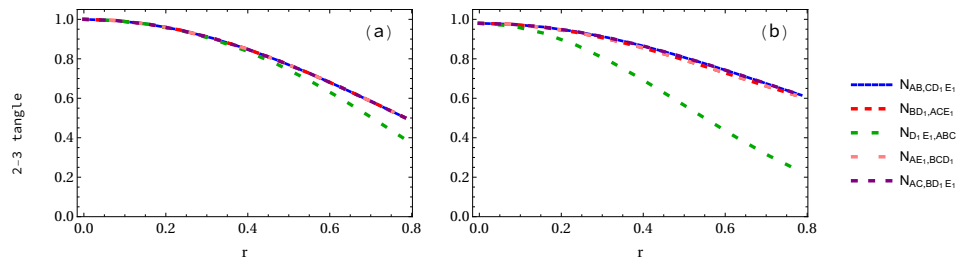

Figure 11. Panels (**a**,**b**) show the 2-3 tangle for both GHZ and W-class states, respectively, when two qubits are accelerated.

When three observers are accelerated (see Figure 12), we notice that the difference among $N_{BD_1,AC_1E_1} = N_{AE_1,BC_1D_1} = N_{AC_1,BD_1E_1}$, $N_{AB,C_1D_1E_1}$ and $N_{D_1E_1,ABC_1}$ is very small in the GHZ state, as shown in Figure 12a, but in the case of W-class state case, as illustrated in Figure 12b, i.e., their difference is big. In the case of GHZ state when $r = \pi/4$, the 2-3 tangle N_{BD_1,AC_1E_1} is 0.353553, but $N_{AB,C_1D_1E_1} = N_{D_1E_1,ABC_1}$ is equal to 0.2965. However, in the W-class state case, as seen in Figure 12b, we find that their difference is obvious, that is, $N_{BD_1,AC_1E_1} = N_{AE_1,BC_1D_1} = N_{AC_1,BD_1E_1} = 0.4566$, $N_{AB,C_1D_1E_1} = 0.2774$ and $N_{D_1E_1,ABC_1} = 0.1873$, respectively.
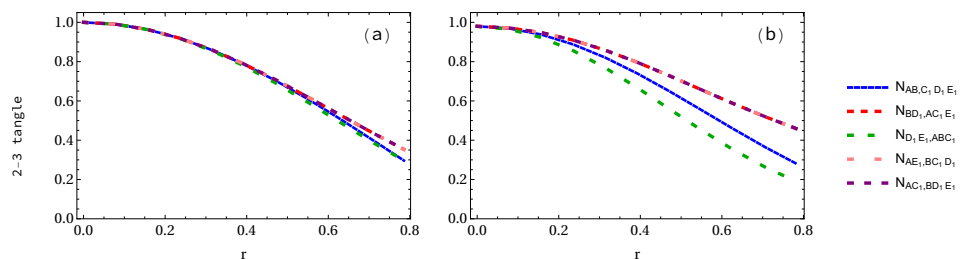

Figure 12. Panels (**a**,**b**) show the 2-3 tangle for both GHZ and W-class states, respectively, when three observers are accelerated.

When four qubits are accelerated, in the case of GHZ state, as displayed in Figure 13a, we find that the difference between $N_{AB_1,C_1D_1E_1} = N_{AE_1,B_1C_1D_1} = N_{AC_1,B_1D_1E_1}$ and $N_{D_1E_1,AB_1C_1} = N_{B_1D_1,AC_1E_1}$ is very small, but in the case of W-class state their difference is a little big. At the infinite limit, the 2-3 tangle is equal to 0.2206 in the case of GHZ state, whereas in the W-class state, the 2-3 tangles $N_{AB_1,C_1D_1E_1} = 0.1976$ and $N_{B_1D_1,AC_1E_1} = 0.1376$, respectively.
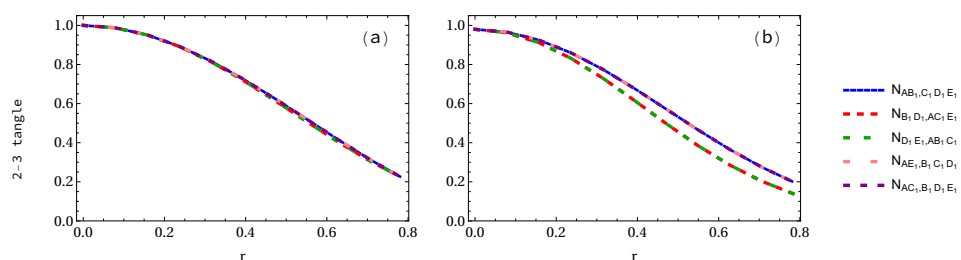

Figure 13. Panels (**a**,**b**) show the 2-3 tangle for both GHZ and W-class states, respectively, when four qubits are accelerated.

Finally, let us consider the case when all the observers are accelerated simultaneously. We see that all 2-3 tangles of either GHZ state or W-class state are equal to each other, as shown in Figure 14. At $r = \pi/4$, the 2-3 tangles of GHZ and W-class states are equal to 0.145527 and approximately 0.05, respectively. The variations of the 2-3 tangles for 1 to 5 arbitrary selected accelerated qubits are displayed in Figure 15. It is found that they all decrease with both the increasing acceleration parameter r and the number of accelerated qubits.
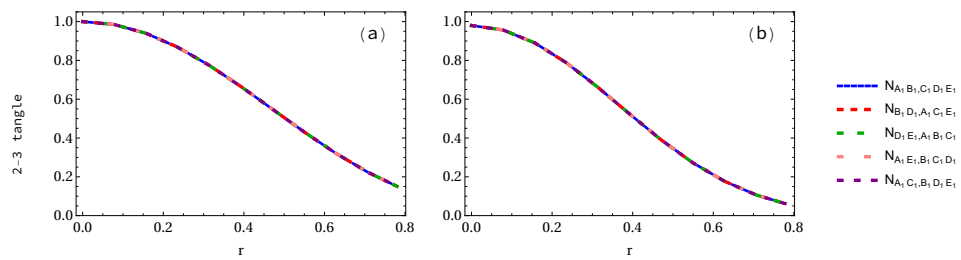

Figure 14. Panels (**a**,**b**) show the 2-3 tangle for both GHZ and W-class states, respectively, when all qubits are accelerated.
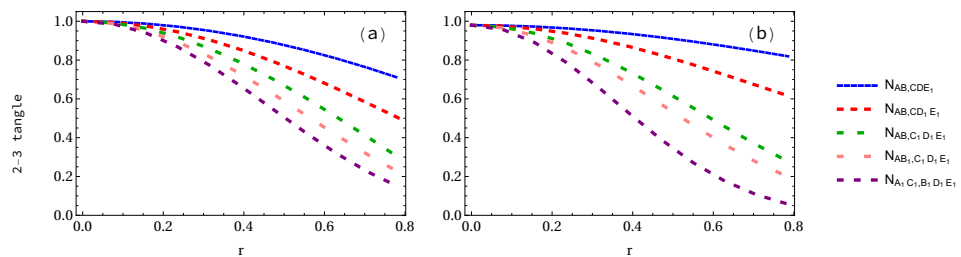

Figure 15. Panels (**a**,**b**) show the 2-3 tangles for both GHZ and W-class states, respectively, when 1 to 5 qubits is (are) accelerated.

3.2. Whole Entanglement Measures

Now, we use the algebraic average π-tangle to describe the multipartite entanglement defined by [50,70]

$$
\begin{aligned}
\pi_A &= N_{A,BCDE}^2 - N_{A,B}^2 - N_{A,C}^2 - N_{A,D}^2 - N_{A,E}^2, \\
\pi_B &= N_{B,ACDE}^2 - N_{B,A}^2 - N_{B,C}^2 - N_{B,D}^2 - N_{B,E}^2, \\
\pi_C &= N_{C,ABDE}^2 - N_{C,A}^2 - N_{C,B}^2 - N_{C,D}^2 - N_{C,E}^2, \\
\pi_D &= N_{D,ABCE}^2 - N_{D,A}^2 - N_{D,B}^2 - N_{D,C}^2 - N_{D,E}^2, \\
\pi_E &= N_{E,ABCD}^2 - N_{E,A}^2 - N_{E,B}^2 - N_{E,C}^2 - N_{E,D}^2,
\end{aligned}
\tag{13}
$$

from which we are able to calculate the whole residual entanglement π_5-tangle defined by $\pi_5 = (\pi_A + \pi_B + \pi_C + \pi_D + \pi_E)/5$. Moreover, we may use another whole residual entanglement measure named as geometric average $\Pi_5 = (\pi_A \cdot \pi_B \cdot \pi_C \cdot \pi_D \cdot \pi_E)^{\frac{1}{5}}$ [71].

Let us first calculate the whole residual entanglement measures π_5 and Π_5 of both GHZ and W-class states and then plot them. In Figure 16a, it is found that the algebraic average π_5 in the GHZ state decreases from 1 to 0.45, 0.2109, 0.1027, 0.0487, and 0.0211 for 1 to 5 arbitrary selected qubits, respectively. In Figure 16b, we show the whole residual entanglement π_5 in the W-class state. It is interesting to note that π_5 decreases from an initial value 0.5813 to 0.3793 (34.73% loss of entanglement), 0.2170 (62.66% loss of entanglement), 0.0994 (82.90% loss of entanglement), 0.0234 (95.95% loss of entanglement), and 0.0035 (99.38% loss of entanglement), respectively.
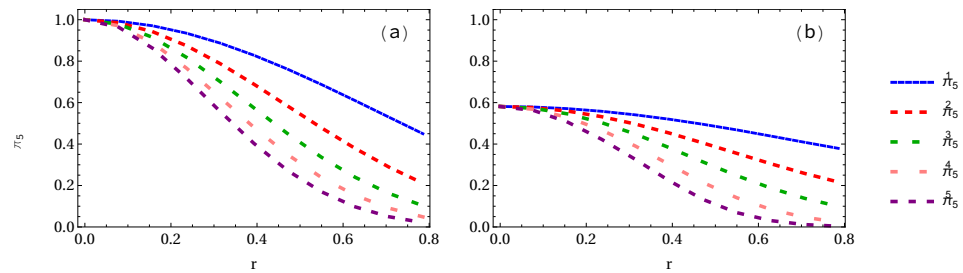
Figure 16. Panels (**a**,**b**) show the whole residual entanglement measure π_5 of GHZ and W-class states, respectively, when 1 to 5 observers is (are) accelerated.

Finally, let us show the variation of the geometric average Π_5 when 1 to 5 accelerated qubits is (are) considered. It is found that Π_5 is very similar to π_5, i.e., whole residual entanglement π_5 and Π_5 are almost same, as shown in Figure 17. To see this clearly, as shown in Figure 18a,b, there is no difference between residual entanglement $\overset{3}{\pi}_5$ and $\overset{3}{\Pi}_5$ in the GHZ state, but there is a very slight difference in the W-class state.
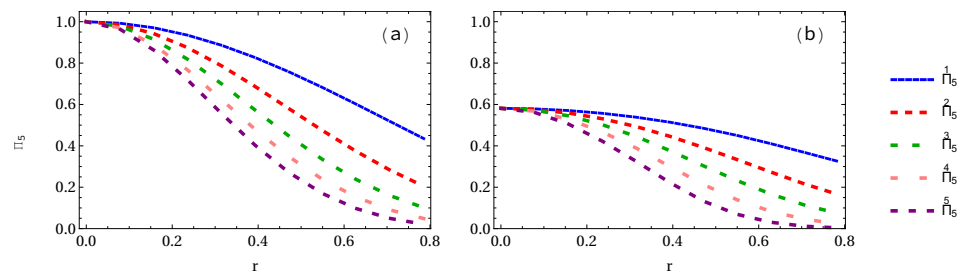

Figure 17. Same as Figure 16 but for the whole entanglement measures Π_5.
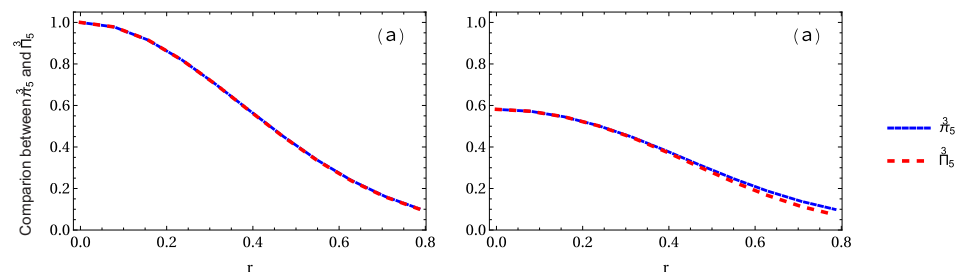

Figure 18. Panels (**a**,**b**) show the difference between whole entanglement measure π_5 when 3 observers are accelerated for the GHZ and W-class states, respectively.

3.3. Entropy

Another useful quantity to measure entanglement is the von Neumann entropy defined by [72–74]:

$$S = -\text{Tr}(\rho \log_2 \rho) = -\sum_{i=1}^{n} \lambda^{(i)} \log_2 \lambda^{(i)}, \tag{14}$$

where $\lambda^{(i)}$ is ith eigenvalue of density matrix ρ. Unlike the negativity, the von Neumann entropy is not required to find the partial transpose of the density matrix except for applying the partial trace to obtain the density matrix of subsystems. We write out explicitly nonzero eigenvalues of GHZ state to calculate entropies in Table 1 but do not list those of W-class state because of complicated expressions.

Table 1. Eigenvalues of GHZ density matrices in the noninertial frame.

Density Matrix	Eigenvalues
ρ_{ABCDE_I}	$\lambda_{31} = \frac{1}{4}(3 + \cos(2r))$ $\lambda_{32} = \frac{\sin^2(r)}{2}$
$\rho_{ABCD_I E_I}$	$\lambda_{29} = \frac{1}{16}(11 + 4\cos(2r) + \cos(4r))$ $\lambda_{30} = \frac{\sin^4(r)}{2}$ $\lambda_{31} = \lambda_{32} = \frac{\sin^2(2r)}{8}$
$\rho_{ABC_I D_I E_I}$	$\lambda_{25} = \frac{1}{64}(15\cos(2r) + 6\cos(4r) + \cos(6r) + 42)$ $\lambda_{26} = \lambda_{27} = \lambda_{28} = \lambda_{29} = \lambda_{30} = \lambda_{31} = \frac{1}{2}\sin^4(r)\cos^2(r)$ $\lambda_{32} = \frac{\sin^6(r)}{2}$
$\rho_{AB_I C_I D_I E_I}$	$\lambda_{17} = \frac{1}{256}(56\cos(2r) + 28\cos(4r) + 8\cos(6r) + \cos(8r) + 163)$ $\lambda_{18} = \lambda_{19} = \lambda_{20} = \lambda_{21} = \frac{1}{2}\sin^2(r)\cos^6(r)$ $\lambda_{22} = \lambda_{23} = \lambda_{24} = \lambda_{25} = \frac{1}{2}\sin^6(r)\cos^2(r)$ $\lambda_{26} = \frac{\sin^8(r)}{2}$ $\lambda_{27} = \lambda_{28} = \lambda_{29} = \lambda_{31} = \lambda_{32} = \frac{1}{32}\sin^4(2r)$
$\rho_{A_I B_I C_I D_I E_I}$	$\lambda_1 = \lambda_2 = \frac{1}{1024}\Big(382 + 120\cos(4r) + 10\cos(8r) +$ $\quad -\sqrt{2}\sqrt{(\cos(4r)+7)^2(511\cos(4r)+62\cos(8r)+\cos(12r)+1474)}\Big)$ $\lambda_3 = \lambda_4 = \lambda_5 = \lambda_6 = \lambda_7 = \lambda_8 = \lambda_9 = \lambda_{10} = \lambda_{11} = \lambda_{12} = \lambda_{13} = \lambda_{14} = \lambda_{15} = \lambda_{16} = \lambda_{17} = \frac{1}{2}\sin^4(r)\cos^6(r)$ $\lambda_{18} = \lambda_{19} = \lambda_{20} = \lambda_{21} = \lambda_{22} = \lambda_{23} = \lambda_{24} = \lambda_{25} = \lambda_{26} = \lambda_{27} = \frac{1}{2}\sin^6(r)\cos^4(r)$ $\lambda_{28} = \lambda_{29} = \lambda_{30} = \lambda_{31} = \lambda_{32} = \frac{1}{2}\sin^8(r)\cos^2(r)$

Let us show the difference of the von Neumann entropy between GHZ and W-class states. As shown in Figure 19, entropy increases as the number of accelerated observers increases. This means that the system becomes more unstable. In the same condition, it is found that von Neumann entropy of the W-class state increases faster than that of GHZ.
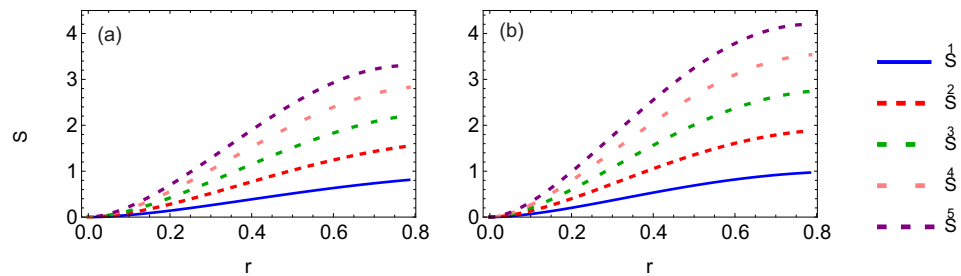

Figure 19. Panels (**a**,**b**) show the von Neumann entropy of the GHZ and W-class states when 1, 2, 3, 4, and all observers are accelerated.

4. Conclusions

In this work, we have studied the entanglement measures of pentapartite GHZ and W-class states by investigating the negativity and whole residual entanglement. We have carried out the cases when the 1, 2, 3, 4, or even all observers are accelerated. As we can see, the degree of entanglement will be degraded when the acceleration parameter r increases. However, we have verified again the fact that the degree of entanglement is dependent of the number of the accelerated particles. That is to say, the degree of the entanglement will decrease faster with the number of accelerated particles. The 1-4 and 2-3 tangles for both GHZ and W-class pentapartite states still exist even if the acceleration tends to infinity. Compared between GHZ and W-class states, we find that the degree of the entanglement of W-class state decreases faster than that of GHZ state when the accelerated parameter increases. The maximum values of the GHZ and W-class states are 1 and 0.8 without the acceleration. For 2-3 tangle case, we notice that when only one particle is accelerated, the GHZ entanglement decays faster than the W-class state, but with the increase of accelerated

particles, the W-class entanglement decays faster than the GHZ state. However, we also note that the 2-3 tangle corresponding to the cases $N_{E_1,ABCD}$ $N_{D_1E_1,ABC}$, $N_{D_1E_1,ABC_1}$ and $N_{D_1E_1,AB_1C_1}$ are always the smallest compared to other cases of the same type if we assume that the acceleration of particles always starts from the rightmost two in A(Alice), B(Bob), C(Charlie), D(David), E(Elly) qubits. The whole entanglement measurements show us that entanglement in GHZ state is greater than that of W-class state. However, we find that there is almost no difference between whole residual entanglements π_5 and Π_5. As far as the von Neumann entropy, compared with the tripartite and tetrapartite entangled systems, the von Neumann entropy of pentapartite system is larger than those of tripartite and tetrapartite cases. As the number of accelerated particles increases, the von Neumann entropy of the system increases accordingly. This implies that the system becomes more and more unstable with the increasing accelerated particles. Before ending this work, we give a useful remark on the difference of the negativity among the tripartite [43], tetrapartite [44], and present pentapartite cases. In the GHZ state case, all 1-1 tangles for them are equal to zero. For the W-class case, however, there only exists a common 1-1 tangle among them. Let us show their difference. For example, the $N_{\alpha,\beta}$ of pentapartite, tetrapartite, and tripartite cases is equal to 0.12111, 0.2071, and 0.412023, respectively, at $r = \pi/4$, but $N_{\alpha_1,\beta}$ of pentapartite and tetrapartite cases will disappear ($N_{\alpha_1,\beta} = 0$) at $r > 0.61548$ and 0.785398, respectively, and $N_{\alpha_1,\beta} = 0.138071$ in the tripartite case at $r = \pi/4$. The N_{α_1,β_1} of pentapartite, tetrapartite, and tripartite cases is equal to 0.38671, 0.472473, and 0.699185, respectively. This implies that the degree of the entanglement decays faster with the increasing entangled particles so that the system becomes more and more unstable.

Author Contributions: Conceptualization, S.-H.D.; methodology, S.-H.D.; software, S.-H.D.; validation, J.L.M.Z., J.R.P., M.A.A. and S.-H.D.; formal analysis, S.-H.D.; investigation, J.L.M.Z. and S.-H.D.; resources, J.L.M.Z. and S.-H.D.; data curation, J.L.M.Z. and S.-H.D.; writing—original draft preparation, J.L.M.Z.; writing—review and editing, S.-H.D.; visualization, J.L.M.Z. and S.-H.D.; supervision, S.-H.D.; project administration, S.-H.D.; funding acquisition, S.-H.D. All authors have read and agreed to the published version of the manuscript.

Institutional Review Board Statement: No applicable.

Informed Consent Statement: Not applicable.

Data Availability Statement: The datasets generated during the current study are available from the corresponding author on reasonable request.

Conflicts of Interest: The authors declare no conflict of interest.

Appendix A. Nonzero Elements of Density Matrices for GHZ and W-Class States in the Noninertial Frame

Table A1. Nonzero entries for GHZ density matrices.

Density Matrix	Nonzero Entries
ρ_{ABCDE_I}	$[1,1] = [2,2] = \frac{1}{2}\cos^2(r)$ $[32,1] = [1,32] = \frac{1}{2}\cos(r)$ $[32,32] = \frac{1}{2}$
$\rho_{ABCD_1E_I}$	$[1,1] = \frac{1}{2}\cos^4(r)$ $[32,1] = [1,32] = \frac{1}{2}\cos^2(r)$ $[2,2] = [3,3] = \frac{1}{8}\sin^2(2r)$ $[4,4] = \frac{1}{2}\sin^4(r)$ $[32,32] = \frac{1}{2}$

Table A1. *Cont.*

Density Matrix	Nonzero Entries
$\rho_{ABC_ID_IE_I}$	$[1,1] = \frac{1}{2}\cos^6(r)$ $[1,32] = [32,1] = \frac{1}{2}\cos^3(r)$ $[2,2] = [3,3] = [5,5] = \frac{1}{2}\cos^4(r)\sin^2(r)$ $[4,4] = [6,6] = [7,7] = \frac{1}{2}\cos^2(r)\sin^4(r)$ $[8,8] = \frac{1}{2}\sin^6(r)$ $[32,32] = \frac{1}{2}$
$\rho_{AB_IC_ID_IE_I}$	$[1,1] = \frac{1}{2}\cos^8(r)$ $[1,32] = [32,1] = \frac{1}{2}\cos^4(r)$ $[2,2] = [3,3] = [5,5] = [9,9] = \frac{1}{2}\cos^6(r)\sin^2(r)$ $[4,4] = [6,6] = [7,7] = [10,10] = [11,11] = [13,13] = \frac{1}{32}\sin^4(2r)$ $[8,8] = [12,12] = [14,14] = [15,15] = \frac{1}{2}\cos^2(r)\sin^6(r)$ $[16,16] = \frac{1}{2}\sin^8(r)$ $[32,32] = \frac{1}{2}$
$\rho_{A_IB_IC_ID_IE_I}$	$[1,1] = \frac{1}{2}\cos^{10}(r)$ $[1,32] = [32,1] = \frac{1}{2}\cos^5(r)$ $[2,2] = [3,3] = [5,5] = [9,9] = [17,17] = \frac{1}{2}\cos^8(r)\sin^2(r)$ $[13,13] = [4,4] = [19,19] = [10,10] = [11,11] = [6,6] = [18,18] = [21,21] = [25,25] = [7,7] = \frac{1}{2}\cos^6(r)\sin^4(r)$ $[8,8] = [12,12] = [14,14] = [15,15] = [20,20] = [22,22] = [23,23] = [26,26] = [27,27] = [29,29] = \frac{1}{2}\cos^4(r)\sin^6(r)$ $[16,16] = [24,24] = [28,28] = [30,30] = [31,31] = \frac{1}{2}\cos^2(r)\sin^8(r)$ $[32,32] = \frac{1}{2} + \frac{1}{2}\sin^{10}(r)$

Table A2. Nonzero entries for pentapartite W-class state.

Density Matrix	Nonzero Entries
ρ_{ABCDE_1}	$[2,2] = \frac{1}{5}$ $[2,3] = [2,5] = [2,9] = [2,17] = [3,2] = [5,2] = [9,2] = [17,2] = \frac{1}{5}\cos(r)$ $[3,3] = [3,5] = [3,9] = [3,17] = [5,3] = [5,5] = [5,9] = [5,17] = [9,3] = [9,5] = [9,9] = [9,17] = [17,3] = [17,5] = [17,9] = [17,17] = \frac{1}{5}\cos^2(r)$ $[4,4], [4,6] = [4,10] = [4,18] = [6,4] = [6,6] = [6,10] = [6,18] = [10,4] = [10,6] = [10,10] = [10,18] = [18,4] = [18,6] = [18,10] = [18,18]$ $= \frac{1}{5}\sin^2(r)$
$\rho_{ABCD_1E_1}$	$[2,2] = [2,3] = [3,2] = [3,3] = \frac{1}{5}\cos^2(r)$ $[2,5] = [2,9] = [2,17] = [3,5] = [3,9] = [3,17] = [5,2] = [5,3] = [9,2] = [9,3] = [17,2] = [17,3] = \frac{1}{5}\cos^3(r)$ $[4,4] = \frac{2}{5}\sin^2(r)$ $[4,6] = [4,7] = [4,10] = [4,11] = [4,18] = [4,19] = [6,4] = [7,4] = [10,4] = [11,4] = [18,4] = [19,4] = \frac{1}{5}\sin^2(r)\cos(r)$ $[5,5] = [5,9] = [5,17] = [9,5] = [9,9] = [9,17] = [17,5] = [17,9] = [17,17] = \frac{1}{5}\cos^4(r)$ $[6,6], [6,10] = [6,18] = [7,7] = [7,11] = [7,19] = [10,6] = [10,10] = [10,18] = [11,7] = [11,11] = [11,19] = [18,6] = [18,10] = [18,18] = [19,7] = [19,11] = [19,19] = \frac{1}{20}\sin^2(2r)$ $[8,8] = [8,12] = [8,20] = [12,8] = [12,12] = [12,20] = [20,8] = [20,12] = [20,20] = \frac{1}{5}\sin^4(r)$
$\rho_{ABC_1D_1E_1}$	$[2,2] = [2,3] = [2,5] = [3,2] = [3,3] = [3,5] = [5,2] = [5,3] = [5,5] = \frac{1}{5}\cos^4(r)$ $[2,9] = [2,17] = [3,9] = [3,17] = [5,9] = [5,17] = [9,2] = [9,3] = [9,5] = [17,2] = [17,3] = [17,5] = \frac{1}{5}\cos^5(r)$ $[4,4] = [6,6] = [7,7] = \frac{1}{10}\sin^2(2r)$ $[4,6] = [4,7] = [6,4] = [6,7] = [7,4] = [7,6] = \frac{1}{20}\sin^2(2r)$ $[4,10] = [4,11] = [4,18] = [4,19] = [6,10] = [6,13] = [6,18] = [6,21] = [7,11] = [7,13] = [7,19] = [7,21] = [10,4] = [10,6] = [11,4] = [11,7] = [13,6] = [13,7] = [18,4] = [18,6] = [19,4] = [19,7] = [21,6] = [21,7] = \frac{1}{5}\sin^2(r)\cos^3(r)$ $[8,8] = \frac{3}{5}\sin^4(r)$ $[8,12], [8,14] = [8,15] = [8,20] = [8,22] = [8,23] = [12,8] = [14,8] = [15,8] = [20,8] = [22,8] = [23,8] = \frac{1}{5}\sin^4(r)\cos(r)$ $[9,9] = [9,17] = [17,9] = [17,17] = \frac{1}{5}\cos^6(r)$ $[10,10], [10,18] = [11,11] = [11,19] = [13,13] = [13,21] = [18,10] = [18,18] = [19,11] = [19,19] = [21,13] = [21,21] = \frac{1}{5}\sin^2(r)\cos^4(r)$ $[12,12] = [12,20] = [14,14] = [14,22] = [15,15] = [15,23] = [20,12] = [20,20] = [22,14] = [22,22] = [23,15] = [23,23] = 1/5\cos(r)^2\sin(r)^4$ $[16,16] = [16,24] = [24,16] = [24,24] = \frac{1}{5}\sin^6(r)$

Table A2. *Cont.*

Density Matrix	Nonzero Entries
$\rho_{AB_1C_1D_1E_1}$	$[2,2] = [2,3] = [2,5] = [2,9] = [3,2] = [3,3] = [3,5] = [3,9] = [5,2] = [5,3] = [5,5] = [5,9] = [9,2] = [9,3] = [9,5] = [9,9] = \frac{1}{5}\cos^6(r)$ $[2,17] = [3,17] = [5,17] = [9,17] = [17,2] = [17,3] = [17,5] = [17,9] = \frac{1}{5}\cos^7(r)$ $[4,4] = [6,6] = [7,7] = [10,10] = [11,11] = [13,13] = \frac{2}{5}\sin^2(r)\cos^4(r)$ $[4,6] = [4,7] = [4,10] = [4,11] = [6,4] = [6,7] = [6,10] = [6,13] = [7,4] = [7,6] = [7,11] = [7,13] = [10,4] = [10,6] = [10,11] = [10,13] = [11,4]$ $= [11,7] = [11,10] = [11,13] = [13,6] = [13,7] = [13,10] = [13,11] = \frac{1}{5}\sin^2(r)\cos^4(r)$ $[4,18] = [4,19] = [6,18] = [6,21] = [7,19] = [7,21] = [10,18] = [10,25] = [11,19] = [11,25] = [13,21] = [13,25] = [18,4] = [18,6] = [18,10] =$ $[19,4] = [19,7] = [19,11] = [21,6] = [21,7] = [21,13] = [25,10] = [25,11] = [25,13] = \frac{1}{5}\sin^2(r)\cos^5(r)$ $[8,8] = [12,12] = [14,14] = [15,15] = \frac{3}{5}\sin^4(r)\cos^2(r)$ $[8,12] = [8,14] = [8,15] = [12,8] = [12,14] = [12,15] = [14,8] = [14,12] = [14,15] = [15,8] = [15,12] = [15,14] = \frac{1}{5}\sin^4(r)\cos^2(r)$ $[8,20] = [8,22] = [8,23] = [12,20] = [12,26] = [12,27] = [14,22] = [14,26] = [14,29] = [15,23] = [15,27] = [15,29] = [20,8] = [20,12] = [22,8] =$ $[22,14] = [23,8] = [23,15] = [26,12] = [26,14] = [27,12] = [27,15] = [29,14] = [29,15] = \frac{1}{5}\sin^4(r)\cos^3(r)$ $[16,16] = \frac{4}{5}\sin^6(r)$ $[16,24] = [16,28] = [16,30] = [16,31] = [24,16] = [28,16] = [30,16] = [31,16] = \frac{1}{5}\sin^6(r)\cos(r)$ $[17,17] = \frac{1}{5}\cos^8(r)$ $[18,18] = [19,19] = [21,21] = [25,25] = \frac{1}{5}\sin^2(r)\cos^6(r)$ $[20,20] = [22,22] = [23,23] = [26,26] = [27,27] = [29,29] = \frac{1}{80}\sin^4(2r)$ $[24,24] = [28,28] = [30,30] = [31,31] = \frac{1}{5}\sin^6(r)\cos^2(r)$ $[32,32] = \frac{1}{5}\sin^8(r)$
$\rho_{A_1B_1C_1D_1E_1}$	$[2,2] = [2,3] = [2,5] = [2,9] = [2,17] = [3,2] = [3,3] = [3,5] = [3,9] = [3,17] = [5,2] = [5,3] = [5,5] = [5,9] = [5,17] = [9,2] = [9,3] = [9,5] =$ $[9,9] = [9,17] = [17,2] = [17,3] = [17,5] = [17,9] = [17,17] = \frac{1}{5}\cos^8(r)$ $[4,4] = [6,6] = [7,7] = [10,10] = [11,11] = [13,13] = [18,18] = [19,19] = [21,21] = [25,25] = \frac{2}{5}\sin^2(r)\cos^6(r)$ $[4,6] = [4,7] = [4,10] = [4,11] = [4,18] = [4,19] = [6,4] = [6,7] = [6,10] = [6,13] = [6,18] = [6,21] = [7,4] = [7,6] = [7,11] = [7,13] = [7,19] =$ $[7,21] = [10,4] = [10,6] = [10,11] = [10,13] = [10,18] = [10,25] = [11,4] = [11,7] = [11,10] = [11,13] = [11,19] = [11,25] = [13,6] = [13,7] =$ $[13,10] = [13,11] = [13,21] = [13,25] = [18,4] = [18,6] = [18,10] = [18,19] = [18,21] = [18,25] = [19,4] = [19,7] = [19,11] = [19,18] = [19,21] =$ $[19,25] = [21,6] = [21,7] = [21,13] = [21,18] = [21,19] = [21,25] = [25,10] = [25,11] = [25,13] = [25,18] = [25,19] = [25,21] = \frac{1}{5}\sin^2(r)\cos^6(r)$ $[8,8], [12,12] = [14,14] = [15,15] = [20,20] = [22,22] = [23,23] = [26,26] = [27,27] = [29,29] = \frac{3}{80}\sin^4(2r)$ $[8,12] = [8,14] = [8,15] = [8,20] = [8,22] = [8,23] = [12,8] = [12,14] = [12,15] = [12,20] = [12,26] = [12,27] = [14,8] = [14,12] = [14,15] =$ $[14,22] = [14,26] = [14,29] = [15,8] = [15,12] = [15,14] = [15,23] = [15,27] = [15,29] = [20,8] = [20,12] = [20,22] = [20,23] = [20,26] = [20,27]$ $= [22,8] = [22,14] = [22,20] = [22,23] = [22,26] = [22,29] = [23,8] = [23,15] = [23,20] = [23,22] = [23,27] = [23,29] = [26,12] = [26,14] =$ $[26,20] = [26,22] = [26,27] = [26,29] = [27,12] = [27,15] = [27,20] = [27,23] = [27,26] = [27,29] = [29,14] = [29,15] = [29,22] = [29,23] =$ $[29,26] = [29,27] = \frac{1}{80}\sin^4(2r)$ $[16,16] = [24,24] = [28,28] = [30,30] = [31,31] = \frac{4}{5}\sin^6(r)\cos^2(r)$ $[16,24] = [16,28] = [16,30] = [16,31] = [24,16] = [24,28] = [24,30] = [24,31] = [28,16] = [28,24] = [28,30] = [28,31] = [30,16] = [30,24] =$ $[30,28] = [30,31] = [31,16] = [31,24] = [31,28] = [31,30] = \frac{1}{5}\sin^6(r)\cos^2(r)$ $[32,32] = \sin^8(r)$

Appendix B. Analytical Expressions of 1-4 Tangles for GHZ and W-Class States

For GHZ state case :

$$N_{E_I,ABCD} = \cos^2(r)$$
$$N_{D,ABCE_I} = N_{C,ABDE_I} = N_{B,ACDE_I} = N_{A,BCDE_I} = \cos(r)$$
$$N_{E_I,ABCD_I} = N_{D_I,ABCE_I} = \frac{1}{16}\left\{-1 + \cos(4r) + 2\sqrt{2}\cos^2(r)\sqrt{35 - 4\cos(2r) + \cos(4r)}\right\}$$
$$N_{C,ABD_IE_I} = N_{B,ACD_IE_I} = N_{A,BCD_IE_I} = \cos^2(r)$$
$$N_{E_I,ABC_ID_I} = \frac{1}{64}\left\{-2 - \cos(2r) + 2\cos(4r) + \cos(6r) + 4\sqrt{2}\cos^3(r)\sqrt{130 - \cos(2r) - 2\cos(4r) + \cos(6r)}\right\}$$
$$N_{B,AC_ID_IE_I} = N_{A,BC_ID_IE_I} = \cos^3(r)$$
$$N_{E_I,AB_IC_ID_I} = \frac{1}{256}\left\{-5 - 4\cos(2r) + 4\cos(4r) + 4\cos(6r) + \cos(8r) + 8\sqrt{2}\cos^4(r)\sqrt{515 - 4\cos(4r) + \cos(8r)}\right\}$$
$$N_{A,B_1C_1D_1E_1} = \frac{1}{256}\left\{56\cos(2r) - 28\cos(4r) + 8\cos(6r) - \cos(8r) + \frac{1}{\sqrt{2}}\Big[45904\cos(2r) + 36680\cos(4r) + 3824\cos(6r)\right.$$
$$\left. + 2844\cos(8r) - 560\cos(10r) + 120\cos(12r) - 16\cos(14r) + \cos(16r) + 42275\Big]^{1/2} - 35\right\}$$
$$N_{E_I,A_IB_IC_ID_I} = \frac{1}{256}\left\{-7 + 4\cos(4r) + 3\cos(8r) + \sqrt{2}\cos^2(r)[11851 + 12532\cos(2r) + 8156\cos(4r) - 116\cos(6r)\right.$$
$$\left. + 436\cos(8r) - 124\cos(10r) + 36\cos(12r) - 4\cos(14r) + \cos(16r)]^{1/2}\right\}$$

<div align="center">For W − class state case :</div>

$$N_{E_I,\mathrm{ABCD}} = \tfrac{1}{5}\left(2\cos(2r) + \sqrt{2}\sqrt{\cos(4r)+7} - 2\right)$$

$$N_{D,\mathrm{ABC}E_I} = N_{C,\mathrm{ABD}E_I} = N_{B,\mathrm{ACD}E_I} = N_{A,\mathrm{BCD}E_I} =$$
$$\tfrac{1}{5}(-2)\mathrm{Root}\Big[32\#1^3 + \#1^2(16\cos(2r) - 16) + \#1(-64\cos(2r) - 12\cos(4r) - 52) +$$
$$+3\cos(2r) - 6\cos(4r) - 3\cos(6r) + 6\&, 1\Big]$$

$$N_{E_I,\mathrm{ABCD}_I} = N_{D_I,\mathrm{ABC}E_I} = \tfrac{1}{10}\mathrm{Root}\Big[2\#1^3 + \#1^2(8\cos(2r) + 3\cos(4r) - 11) + \#1(-64\cos(2r) +$$
$$-28\cos(4r) - 36) + 12\cos(2r) - 12\cos(4r) - 12\cos(6r) - 3\cos(8r) + 15\&, 1\Big]$$

$$N_{C,\mathrm{ABD}_I E_I} = N_{B,\mathrm{ACD}_I E_I} = N_{A,\mathrm{BCD}_I E_I} = \tfrac{1}{10}\mathrm{Root}\Big[16\#1^3 + \#1^2(8\cos(4r) - 8) +$$
$$+\#1(-464\cos(2r) - 208\cos(4r) - 48\cos(6r) - 4\cos(8r) - 300) + 48\cos(2r) +$$
$$-15\cos(4r) - 40\cos(6r) - 26\cos(8r) - 8\cos(10r) - \cos(12r) + 42\&, 1\Big]$$

$$N_{E_I,\mathrm{ABC}_I D_I} = N_{D_1,\mathrm{ABC}_1 E_I} = N_{C_1,\mathrm{ABD}_1 E_1} = \tfrac{1}{10}\Big|\mathrm{Root}\Big[64\#1^3 + (-16\cos(2r) + 128\cos(4r) +$$
$$+16\cos(6r) - 128)\#1^2 + (-1728\cos(2r) - 960\cos(4r) - 320\cos(6r) +$$
$$-48\cos(8r) - 1040)\#1 + 165\cos(2r) - 22\cos(4r) - 121\cos(6r) - 100\cos(8r)$$
$$-43\cos(10r) - 10\cos(12r) - \cos(14r) + 132\&, 1\Big]\Big|$$

$$N_{B,\mathrm{AC}_I D_I E_I} = N_{A,\mathrm{BC}_I D_I E_I} = -\tfrac{1}{10}\mathrm{Root}\Big[2048\#1^3 + \#1^2(-256\cos(2r) + 512\cos(4r) +$$
$$+256\cos(6r) - 512) + \#1(-52992\cos(2r) - 30960\cos(4r) - 12160\cos(6r) +$$
$$-2976\cos(8r) - 384\cos(10r) - 16\cos(12r) - 31584) + 2002\cos(2r) + 208\cos(4r) +$$
$$-1092\cos(6r) - 1288\cos(8r) - 820\cos(10r) - 336\cos(12r) +$$
$$-89\cos(14r) - 14\cos(16r) - \cos(18r) + 1430\&, 1\Big]$$

$$N_{A,B_1 C_1 D_1 E_1} = \tfrac{1}{640}\Big(\big|4\cos(2r) - 4\cos(4r) - 4\cos(6r) - \cos(8r) +$$
$$-32\sqrt{2}\sqrt{\cos^{12}(r)(60\cos(2r) + \cos(4r) + 67)} + 5\big| + \big|240\cos(2r) + 92\cos(4r) +$$
$$+16\cos(6r) + \cos(8r) +$$
$$-8\sqrt{2}\sqrt{\cos^{8}(r)(904\cos(2r) + 156\cos(4r) + 56\cos(6r) + \cos(8r) + 931)} + 163\big|\Big)$$

$$N_{A_1,B_1 C_1 D_1 E_1} = N_{E_I,A_I B_I C_I D_I} = N_{D_1,\mathrm{AB}_1 C_1 E_1} = N_{C_1,\mathrm{AB}_1 D_1 E_1} = N_{B_1,\mathrm{AC}_1 D_1 E_1} =$$
$$\tfrac{1}{640}\big|20\cos(2r) - 20\cos(4r) - 20\cos(6r) - 5\cos(8r) +$$
$$-32\sqrt{2}\sqrt{\cos^{12}(r)(41(\cos(4r)+3) - 36\cos(2r))} + 25\big|$$

Appendix C. Analytical Expressions of 2-3 Tangles for GHZ and W-Class States

<div align="center">For GHZ state case :</div>

$$N_{\mathrm{AB,CDE}_I} = N_{\mathrm{AD,BCE}_I} = N_{\mathrm{CD,ABE}_I} = N_{\mathrm{BE}_I,\mathrm{ACD}} = N_{\mathrm{AE}_I,\mathrm{BCD}} = \cos(r)$$

$$N_{\mathrm{AB,CD}_I E_I} = N_{\mathrm{CE}_I,\mathrm{ABD}_I} = N_{\mathrm{AE}_I,\mathrm{BCD}_I} = N_{\mathrm{BD}_I,\mathrm{ACE}} = \cos^2(r)$$

$$N_{D_I E_I,\mathrm{ABC}} = \tfrac{1}{16}\left\{-3 + 4\cos(2r) - \cos[4r] + \frac{\sqrt{227 + 200\cos(2r) + 92\cos(4r) - 8\cos(6r) + \cos(8r)}}{\sqrt{2}}\right\}$$

$$N_{\mathrm{AB},C_I D_I E_I} = \tfrac{1}{64}\Big\{-10 + 15\cos(2r) - 6\cos(4r) + \cos(6r) + \tfrac{1}{\sqrt{2}}\big[3022 + 3048\cos(2r) + 2031\cos(4r)$$
$$+36\cos(6r) + 66\cos(8r) - 12\cos(10r) + \cos(12r)\big]^{1/2}\Big\}$$

$$N_{\mathrm{AE}_I,\mathrm{BC}_I D_I} = N_{\mathrm{BE}_I,\mathrm{AC}_I D_I} = \cos^3(r)$$

$$N_{D_I E_I,\mathrm{ABC}_I} = \tfrac{1}{64}\Big\{-2 + \cos(2r) + 2\cos(4r) - \cos(6r)$$
$$+2\sqrt{2}\cos^2(r)\sqrt{291 + 200\cos(2r) + 28\cos(4r) - 8\cos(6r) + \cos(8r)}\Big\}$$

$$N_{\mathrm{AB}_I,C_I D_I E_I} = \tfrac{1}{256}\Big\{-5 + 4\cos(2r) + 4\cos(4r) - 4\cos(6r) + \cos(8r) + 2\sqrt{2}\cos^2(r)\big[3534 + 3304\cos(2r)$$
$$+1519\cos(4r) - 220\cos(6r) + 66\cos(8r) - 12\cos(10r) + \cos(12r)\big]^{1/2}\Big\}$$

$$N_{B_I E_I,\mathrm{AC}_I D_I} = \tfrac{1}{256}\Big\{-3 + 4\cos(4r) - \cos(8r) + 8\sqrt{2}\cos^4(r)\sqrt{547 - 56\cos(2r) + 28\cos(4r) - 8\cos(6r) + \cos(8r)}\Big\}$$

$$N_{A_I B_I,C_I D_I E_I} = \tfrac{1}{256}\Big\{-3 + 4\cos(4r) - \cos(8r) + 4\sqrt{2}\cos^4(r)[1122 + 848\cos(2r) + 127\cos(4r)$$
$$-72\cos(6r) + 30\cos(8r) - 8\cos(10r) + \cos(12r)]^{1/2}\Big\}$$

For W − class state case :

$$N_{\mathrm{AB,CDE}_I} = N_{\mathrm{AD,BCE}_I} = N_{\mathrm{CD,ABE}_I} = \tfrac{1}{5}(-2)\mathrm{Root}\Big[4\#1^3 + \#1^2(4\cos(2r)-4)+$$
$$\#1(-12\cos(2r)-2\cos(4r)-10)+\cos(2r)-2\cos(4r)-\cos(6r)+2\&,1\Big]$$

$$N_{\mathrm{BE}_I,\mathrm{ACD}} = N_{\mathrm{AE}_I,\mathrm{BCD}} = \tfrac{1}{5}(-2)\mathrm{Root}\Big[32\#1^3 + \#1^2(48\cos(2r)-48)+$$
$$\#1(-96\cos(2r)-12\cos(4r)-84)+9\cos(2r)-18\cos(4r)-9\cos(6r)+18\&,1\Big]$$

$$N_{\mathrm{AB,CD}_I E_I} = \tfrac{1}{10}\mathrm{Root}\Big[8\#1^3 + \#1^2(8\cos(4r)-8)+\#1(-352\cos(2r)+$$
$$-152\cos(4r)-32\cos(6r)-2\cos(8r)-230)+48\cos(2r)-15\cos(4r)+$$
$$-40\cos(6r)-26\cos(8r)-8\cos(10r)-\cos(12r)+42\&,1\Big]$$

$$N_{\mathrm{CE}_I,\mathrm{ABD}} = N_{\mathrm{AE}_I,\mathrm{BCD}_I} = N_{\mathrm{BD}_I,\mathrm{ACE}} = -\tfrac{1}{10}\mathrm{Root}\Big[256\#1^6 + \#1^5(1024\cos(2r)+$$
$$+384\cos(4r)-1408)+\#1^4(-8192\cos(2r)-7424\cos(4r)-64\cos(8r)-8896)+$$
$$\#1^3(5120\cos(2r)-5024\cos(4r)-4864\cos(6r)-4416\cos(8r)-256\cos(10r)+$$
$$-96\cos(12r)+9536)+\#1^2(-2048\cos(2r)+2432\cos(4r)+3072\cos(6r)+$$
$$+1440\cos(8r)-1024\cos(10r)-896\cos(12r)-8\cos(16r)-2968)+$$
$$+\#1(224\cos(2r)+3052\cos(4r)-448\cos(6r)-1616\cos(8r)+320\cos(10r)+$$
$$+526\cos(12r)-112\cos(14r)-92\cos(16r)+16\cos(18r)+6\cos(20r)-1876)+$$
$$-792\cos(4r)+495\cos(8r)-220\cos(12r)+66\cos(16r)-12\cos(20r)+\cos(24r)+462\&,1\Big]$$

$$N_{D_I E_I,\mathrm{ABC}} = \tfrac{1}{40}\Big(2\sqrt{6}\sqrt{\cos^4(r)(20\cos(2r)+3\cos(4r)+41)}+3\cos(4r)-3\Big)$$

$$N_{\mathrm{AB},C_I D_I E_I} = \tfrac{1}{80}\Big|\cos(2r)-2\cos(4r)-\cos(6r)-8\sqrt{2}\sqrt{\cos^8(r)(20\cos(2r)+\cos(4r)+27)}+2\Big|$$

$$N_{\mathrm{AE}_I,\mathrm{BC}_I D_I} = N_{\mathrm{BE}_I,\mathrm{AC}_I D_I} = -\tfrac{1}{10}\mathrm{Root}\Big[134217728\#1^7 + \#1^6(218103808\cos(2r)+$$
$$+167772160\cos(4r)+50331648\cos(6r)-436207616)+\#1^5(-5385486336\cos(2r)+$$
$$+ -3138387968\cos(4r)-1048576000\cos(6r)-224395264\cos(8r)+$$
$$-8388608\cos(10r)+1048576\cos(12r)-3080716288)+\#1^4(2032795648\cos(2r)+$$
$$-248512512\cos(4r)-1369702400\cos(6r)-1225261056\cos(8r)+$$
$$-619970560\cos(10r)-196083712\cos(12r)-42795008\cos(14r)+$$
$$-4063232\cos(16r)-327680\cos(18r)+1673920512)+\#1^3(-312737792\cos(2r)+$$
$$+157515776\cos(4r)+343670784\cos(6r)+234180608\cos(8r)+$$
$$+42336256\cos(10r)-67977216\cos(12r)-65667072\cos(14r)+$$
$$-27828224\cos(16r)-7471104\cos(18r)-1458176\cos(20r)-131072\cos(22r)+$$
$$-20480\cos(24r)-294412288)+\#1^2(-17313024\cos(2r)+62495232\cos(4r)+$$
$$+36309248\cos(6r)-27261952\cos(8r)-28723456\cos(10r)+3595776\cos(12r)+$$
$$+11975936\cos(14r)+2299904\cos(16r)-2281728\cos(18r)-1091072\cos(20r)+$$
$$-21248\cos(22r)+113664\cos(24r)+54016\cos(26r)+11776\cos(28r)+$$
$$+256\cos(30r)-40163328)+\#1(3010304\cos(2r)-12497760\cos(4r)+$$
$$-6544384\cos(6r)+6131968\cos(8r)+5596160\cos(10r)-1353536\cos(12r)+$$
$$-2677248\cos(14r)-259712\cos(16r)+665088\cos(18r)+228800\cos(20r)+$$
$$-33792\cos(22r)-30976\cos(24r)-17408\cos(26r)-9040\cos(28r)+640\cos(30r)+$$
$$+2208\cos(32r)+640\cos(34r)+48\cos(36r)+7788000)-60996\cos(2r)+$$
$$+392496\cos(4r)+148954\cos(6r)-262548\cos(8r)-163710\cos(10r)+$$
$$128928\cos(12r)+121176\cos(14r)-41616\cos(16r)-64872\cos(18r)+$$
$$4896\cos(20r)+25245\cos(22r)+2958\cos(24r)-6903\cos(26r)-1944\cos(28r)+$$
$$+1210\cos(30r)+564\cos(32r)-102\cos(34r)-88\cos(36r)-3\cos(38r)+$$
$$6\cos(40r)+\cos(42r)-223652\&,1\Big]$$

$$N_{D_I E_I,\mathrm{ABC}_I} = N_{C_1 D_1,\mathrm{ABE}_1} = -\tfrac{1}{10}\mathrm{Root}\Big[64\#1^3 + \#1^2(224\cos(2r)+32\cos(4r)+32\cos(6r)+$$
$$-288)+\#1(-2632\cos(2r)-1538\cos(4r)-436\cos(6r)-100\cos(8r)+$$
$$-4\cos(10r)+2\cos(12r)-1436)+690\cos(2r)-212\cos(4r)-538\cos(6r)+$$
$$-356\cos(8r)-142\cos(10r)-44\cos(12r)-10\cos(14r)-\cos(16r)+613\&,1\Big]$$

$$N_{\mathrm{AB}_I,C_I D_I E_I} = N_{\mathrm{AD}_1,B_1 C_1 E_1} = \frac{1}{40}\Big|\mathrm{Root}\Big[2048\#1^4 + (-4096\cos(2r) + 10240\cos(4r) +$$
$$+4096\cos(6r) + 512\cos(8r) - 10752)\#1^3 + (-1179648\cos(2r) +$$
$$-772736\cos(4r) - 368640\cos(6r) - 120896\cos(8r) - 24576\cos(10r) - 2432\cos(12r) +$$
$$+16\cos(16r) - 676816)\#1^2 + (1036320\cos(2r) + 163200\cos(4r) +$$
$$-499872\cos(6r) - 648192\cos(8r) - 457296\cos(10r) - 220224\cos(12r) +$$
$$-76016\cos(14r) - 18688\cos(16r) - 3120\cos(18r) - 320\cos(20r) - 16\cos(22r) +$$
$$+724224)\#1 + 15504\cos(2r) - 22287\cos(4r) - 27588\cos(6r) - 3534\cos(8r) +$$
$$+13740\cos(10r) + 10011\cos(12r) - 168\cos(14r) - 3732\cos(16r) - 1896\cos(18r) +$$
$$-15\cos(20r) + 372\cos(22r) + 174\cos(24r) + 36\cos(26r) + 3\cos(28r) + 19380\&, 1\Big]\Big|$$

$$N_{B_1 E_I,AC_I D_I} = N_{D_1 E_1,\mathrm{AB}_1 C_1} = N_{B_1 C_1,\mathrm{AD}_1 E_1} = \frac{1}{40}\Big|\mathrm{Root}\Big[512\#1^4 + (14336\cos(2r) +$$
$$-3584\cos(4r) + 2048\cos(6r) + 128\cos(8r) - 12928)\#1^3 + (-309888\cos(2r) +$$
$$-208864\cos(4r) - 75648\cos(6r) - 29072\cos(8r) - 7808\cos(10r) - 288\cos(12r) +$$
$$+128\cos(14r) + 4\cos(16r) - 154996)\#1^2 + (145024\cos(2r) - 23680\cos(4r) +$$
$$-107264\cos(6r) - 68608\cos(8r) - 25344\cos(10r) - 17216\cos(12r) - 11328\cos(14r) +$$
$$-4352\cos(16r) - 1088\cos(18r) - 64\cos(20r) + 113920)\#1 - 15184\cos(2r) +$$
$$+39941\cos(4r) + 28724\cos(6r) - 10566\cos(8r) - 17660\cos(10r) - 2953\cos(12r) +$$
$$+3976\cos(14r) + 2204\cos(16r) + 328\cos(18r) - 123\cos(20r) - 164\cos(22r) +$$
$$-90\cos(24r) - 20\cos(26r) - \cos(28r) - 28412\&, 1\Big]\Big|$$

$$N_{A_1 B_I,C_I D_I E_I} = N_{B_1 D_1,A_1 C_1 E_1} = N_{D_1 E_1,A_1 B_1 C_1} = \frac{1}{40}\Big|\mathrm{Root}\Big[512\#1^3 + (256\cos(2r) +$$
$$+2816\cos(4r) - 256\cos(6r) + 704\cos(8r) - 3520)\#1^2 + (-274560\cos(2r) +$$
$$-197120\cos(4r) - 104832\cos(6r) - 41216\cos(8r) - 13440\cos(10r) +$$
$$-3584\cos(12r) - 384\cos(14r) + 64\cos(16r) - 151360)\#1 +$$
$$+18360\cos(2r) - 18360\cos(4r) - 28152\cos(6r) - 9639\cos(8r) + 8100\cos(10r) +$$
$$+9684\cos(12r) + 3132\cos(14r) - 1026\cos(16r) - 1332\cos(18r) - 540\cos(20r) +$$
$$-108\cos(22r) - 9\cos(24r) + 19890\&, 1\Big]\Big|$$

References

1. Bennett, C.H.; Brassard, G.; Crépeau, C.; Jozsa, R.; Peres, A.; Wootters, W.K. Teleporting an unknown quantum state via dual classical and Einstein-Podolsky-Rosen channels. *Phys. Rev. Lett.* **1993**, *70*, 1895. [CrossRef]
2. Bennett, C.H.; Bernstein, E.; Brassard, G.; Vazirani, U. Strengths and weaknesses of quantum computing. *SIAM J. Comput.* **1997**, *26*, 1510. [CrossRef]
3. Bouwmeester, D.; Ekert, A.; Zeilinger, A. The physics of quantum information: Basic concepts. In *The Physics of Quantum Information*; Springer: Berlin, Germany, 2000.
4. Nielsen, M.A.; Chuang, I.L. Quantum Computation and Quantum Information. *Phys. Today* **2010**, *54*, 60.
5. Fuchs, C.A.; Gisin, N.; Griffiths, R.B.; Niu, C.S.; Peres, A. Optimal eavesdropping in quantum cryptography. I. Information bound and optimal strategy. *Phys. Rev. A* **1997**, *56*, 1163. [CrossRef]
6. Vidal, G. Efficient classical simulation of slightly entangled quantum computations. Quantum coherence and entanglement partitions for two driven quantum dots inside a coherent micro cavity. *Phys. Rev. Lett.* **2003**, *91*, 147902. [CrossRef]
7. Mohamed, A.B.A.; Eleuch, H.; Raymond Ooi, C.H. Quantum coherence and entanglement partitions for two driven quantum dots inside a coherent micro cavity. *Phys. Lett. A* **2019**, *383*, 125905. [CrossRef]
8. Mohamed, A.B.A.; Eleuch, H. Coherence and information dynamics of a Λ-type three-level atom interacting with a damped cavity field. *Eur. Phys. J. Plus* **2017**, *132*, 75. [CrossRef]
9. Asjad, M.; Qasymeh, M.; Eleuch, H. Continuous-Variable Quantum Teleportation Using a Microwave-Enabled Plasmonic Graphene Waveguide. *Phys. Rev. Appl.* **2021**, *16*, 034046. [CrossRef]
10. Eleuch, H.; Rotter, I. Nearby states in non-Hermitian quantum systems I: Two states. *Eur. Phys. J. D* **2015**, *69*, 229. [CrossRef]
11. Shor, P.W. Algorithms for Quantum Computation: Discrete Logarithms and Factoring. In Proceedings of the 35th Annual Symposium on Foundations of Computer Science, Los Alamitos, CA, USA, 20–22 November 1994; p. 124.
12. Grover, L.K. Quantum Mechanics Helps in Searching for a Needle in a Haystack. *Phys. Rev. Lett.* **1997**, *79*, 325. [CrossRef]
13. Augusiak, R.; Horodecki, P. Multipartite secret key distillation and bound entanglement. *Phys. Rev. A* **2009**, *80*, 042307. [CrossRef]
14. Alsing, P.M.; Milburn, G.J. Teleportation with a uniformly accelerated partner. *Phys. Rev. Lett.* **2003**, *91*, 180404. [CrossRef] [PubMed]
15. Wang, J.; Jing, J. Multipartite entanglement of fermionic systems in noninertial frames. *Phys. Rev. A* **2011**, *83*, 022314; Erratum in *Phys. Rev. A* **2018**, *97*, 029902. [CrossRef]

16. Alsing, P.M.; Fuentes-Schuller, I.; Mann, R.B.; Tessier, T.E. Entanglement of Dirac fields in noninertial frames. *Phys. Rev. A* **2006**, *74*, 032326. [CrossRef]
17. Peres, A. Terno, D.R. Quantum information and relativity theory. *Rev. Mod. Phys.* **2004**, *76*, 93. [CrossRef]
18. Crispino, L.C.B.; Higuchi, A.; Matsa, G.E.A. The Unruh effect and its applications. *Rev. Mod. Phys.* **2008**, *80*, 787. [CrossRef]
19. Davies, P.C.W. Scalar production in Schwarzschild and Rindler metrics. *J. Phys. A Math. Gen.* **1975**, *8*, 609. [CrossRef]
20. Unruh, W.G. Notes on black-hole evaporation. *Phys. Rev. D* **1976**, *14*, 870. [CrossRef]
21. Bruschi, D.E.; Louko, J.; Martín-Martínez, E.; Dragan, A.; Fuentes, I. Unruh effect in quantum information beyond the single-mode approximation. *Phys. Rev. A* **2010**, *82*, 042332. [CrossRef]
22. Landulfo, A.G.S.; Matsas, G. Sudden death of entanglement and teleportation fidelity loss via the Unruh effect. *Phys. Rev. A* **2009**, *80*, 032315. [CrossRef]
23. Qiang, W.C.; Sun, G.H.; Dong, Q.; Camacho-Nieto, O.; Dong, S.H. Concurrence of three Jaynes–Cummings systems. *Quantum Inf. Process.* **2018**, *17*, 90. [CrossRef]
24. Qiang, W.C.; Sun, G.H.; Dong, Q.; Dong, S.H. Genuine multipartite concurrence for entanglement of Dirac fields in noninertial frames. *Phys. Rev. A* **2018**, *98*, 022320. [CrossRef]
25. Hwang, M.R.; Park, D.; Jung, E. Tripartite entanglement in a noninertial frame. *Phys. Rev. A* **2011**, *83*, 012111. [CrossRef]
26. Yao, Y.; Xiao, X.; Ge, L.; Wang, X.G.; Sun, C.P. Quantum Fisher information in noninertial frames. *Phys. Rev. A* **2014**, *89*, 042336. [CrossRef]
27. Khan, S. Tripartite entanglement of fermionic system in accelerated frames. *Ann. Phys.* **2014**, *348*, 270. [CrossRef]
28. Khan, S.; Khan, N.A.; Khan, M.K. Non-maximal tripartite entanglement degradation of Dirac and scalar fields in non-inertial frames. *Commun. Theor. Phys.* **2014**, *61*, 281. [CrossRef]
29. Bruschi, D.E.; Dragan, A.; Fuentes, I.; Louko, J. Particle and antiparticle bosonic entanglement in noninertial frames. *Phys. Rev. D* **2012**, *86*, 025026. [CrossRef]
30. Martín-Martínez, E.; Fuentes, I. Redistribution of particle and antiparticle entanglement in noninertial frames. *Phys. Rev. A* **2011**, *83*, 052306. [CrossRef]
31. Friis, N.; Lee, A.R.; Bruschi, D.E. Fermionic-mode entanglement in quantum information. *Phys. Rev. A* **2013**, *87*, 022338. [CrossRef]
32. Smith, A.; Mann, R.B. Persistence of tripartite nonlocality for noninertial observers. *Phys. Rev. A* **2012**, 86, 012306. [CrossRef]
33. Moradpour, H.; Maghool, S.; Moosavi, S.A. Three-particle Bell-like inequalities under Lorentz transformations. *Quantum Inf. Process.* **2015**, *14*, 3913. [CrossRef]
34. Moradi, S.; Amiri, F. Nonlocality and multipartite entanglement in asymptotically flat space-times. *Commun. Theor. Phys.* **2016**, *65*, 17. [CrossRef]
35. Fuentes-Schuller, I.; Mann, R.B. Alice falls into a black hole: Entanglement in noninertial frames. *Phys. Rev. Lett.* **2005**, *95*, 120404. [CrossRef] [PubMed]
36. Ou, Y.C.; Fan, H. Monogamy inequality in terms of negativity for three-qubit states. *Phys. Rev. A* **2007**, *75*, 062308. [CrossRef]
37. Park, D.K. Tripartite entanglement-dependence of tripartite non-locality in non-inertial frames. *J. Phys. A* **2012**, *45*, 415308. [CrossRef]
38. Hwang, M.R.; Jung, E.; Park, D.K. Three-tangle in non-inertial frame. *Class. Quant. Grav.* **2012**, *29*, 224004. [CrossRef]
39. Park, D.K. Tripartite entanglement dynamics in the presence of Markovian or non-Markovian environment. *Quantum Inf. Process.* **2016**, *15*, 3189. [CrossRef]
40. Gartzke, S.; Osterloh, A. Generalized W state of four qubits with exclusively the three-tangle. *Phys. Rev. A* **2018**, *98*, 052307. [CrossRef]
41. Peng, X.H.; Suter, D. Spin qubits for quantum simulations. *Front. Phys. China* **2010**, *5*, 1. [CrossRef]
42. Torres-Arenas, A.J.; López-Zúñiga, E.O.; Saldaña-Herrera, J.A.; Dong, Q.; Sun, G.H.; Dong, S.H. Tetrapartite entanglement measures of W-class in noninertial frames. *Chin. Phys. B* **2019**, *28*, 070301. [CrossRef]
43. Torres-Arenas, A.J.; Dong, Q.; Sun, G.H.; Qiang, W.C.; Dong, S.H. Entanglement measures of W-state in noninertial frames. *Phys. Lett. B* **2019**, *789*, 93. [CrossRef]
44. Dong, Q.; Torres-Arenas, A.J.; Sun, G.H.; Dong, S.H. Tetrapartite entanglement features of W-Class state in uniform acceleration. *Front. Phys.* **2020**, *15*, 11602. [CrossRef]
45. Dong, Q.; Sánchez-Manilla, A.A.; López-Yáñez, I.; Sun, G.H.; Dong, S.H. Tetrapartite entanglement measures of GHZ state with uniform acceleration. *Phys. Scr.* **2019**, *94*, 105101. [CrossRef]
46. Dong, Q.; Mercado Sanchez, M.A.; Sun, G.H.; Toutounji, M.; Dong, S.H. Tripartite entanglement measures of generalized GHZ state in uniform acceleration. *Chin. Phys. Lett.* **2019**, *36*, 100301. [CrossRef]
47. Dong, Q.; Sun, G.H.; Toutounji, M.; Dong, S.H. Tetrapartite entanglement measures of GHZ state with nonuniform acceleration. *Optik* **2020**, *201*, 163487. [CrossRef]
48. Dong, Q.; Santana Carrillo, R.; Sun, G.H.; Dong, S.H. Tetrapartite entanglement measures of generalized GHZ state in the noninertial frames. *Chin. Phys. B* **2022**, *31*, 030303. [CrossRef]
49. Sun, W.Y.; Wang, D.; Yang, J.; Ye, L. Enhancement of multipartite entanglement in an open system under non-inertial frames. *Quantum Inf. Process.* **2017**, *16*, 90. [CrossRef]
50. Coffman, V.; Kundu, J.; Wooters, W.K. Distributed entanglement. *Phys. Rev. A* **2000**, *61*, 052306. [CrossRef]

51. Mejía Ocampo, D.; Salgado Ramírez, J.C.; Yáñez-Márquez, C.; Sun, G.H. Entanglement measures of a pentapartite W-class state in the noninertial frame. *Quantum Inf. Process.* **2022**, *21*, 46.
52. Dür, W.; Vidal, G.; Cirac, J.I. Three qubits can be entangled in two inequivalent ways. *Phys. Rev. A* **2000**, *62*, 062314. [CrossRef]
53. Socolovsky, M. Rindler space and Unruh effect. *arXiv* **2013**, arXiv:1304.2833.
54. Nakahara, M.; Wan, Y.; Sasaki, Y. *Diversities in Quantum Computation and Quantum Information*; World Scientific: Singapore, 2013.
55. Birrel, N.D.; Davies, P.C.W. *Quantum Fields in Curved Space*; Cambridge University: Cambridge, UK, 1982.
56. Qiang, W.C.; Zhang, L. Geometric measure of quantum discord for entanglement of Dirac fields in noninertial frames. *Phys. Lett. B* **2015**, *742*, 383. [CrossRef]
57. Dong, Q.; Torres-Arenas, A.J.; Sun, G.H.; Qiang, W.C.; Dong, S.H. Entanglement measures of a new type pseudo-pure state in accelerated frames. *Front. Phys.* **2019**, *14*, 21603. [CrossRef]
58. Mehri-Dehnavi, H.; Mirza, B.; Mohammadzadeh, H.; Rahimi, R. Pseudo-entanglement evaluated in noninertial frames. *Ann. Phys.* **2011**, *326*, 1320. [CrossRef]
59. Doukas, J.; Brown, E.G.; Dragan, A.; Mann, R.B. Entanglement and discord: Accelerated observations of local and global modes. *Phys. Rev. A* **2013**, *87*, 012306. [CrossRef]
60. Martín-Martínez, E.; Garay, L.J.; León, J. Unveiling quantum entanglement degradation near a Schwarzschild black hole. *Phys. Rev. D* **2010**, *82*, 064006. [CrossRef]
61. Martín-Martínez, E.; Garay, L.J.; León, J. Quantum entanglement produced in the formation of a black hole. *Phys. Rev. D* **2010**, *82*, 064028. [CrossRef]
62. Martín-Martínez, E.; Hosler, D.; Montero, M. Fundamental limitations to information transfer in accelerated frames. *Phys. Rev. A* **2012**, *86*, 062307. [CrossRef]
63. Dragan, A.; Doukas, J.; Martín-Martínez, E.; Edward Bruschi, D. Localized projective measurement of a quantum field in non-inertial frames. *Class. Quantum Grav.* **2013**, *30*, 235006. [CrossRef]
64. Dragan, A.; Doukas, J.; Martín-Martínez, E. Localized detection of quantum entanglement through the event horizon. *Phys. Rev. A* **2013**, *87*, 052326. [CrossRef]
65. Alsing, P.M.; Fuentes, I. Observer-dependent entanglement. *Class. Quantum Grav.* **2012**, *29*, 224001. [CrossRef]
66. Choi, J.H.; Kim, J.S. Negativity and strong monogamy of multiparty quantum entanglement beyond qubits. *Phys. Rev. A* **2015**, *92*, 042307. [CrossRef]
67. Vidal, G.; Werner, R.F. Computable measure of entanglement. *Phys. Rev. A* **2002**, *65*, 032314. [CrossRef]
68. Li, Y.; Liu, C.; Wang, Q.; Zhang, H.; Hu, L. Tetrapartite entanglement of fermionic systems in noninertial frames. *Optik* **2016**, *127*, 9788. [CrossRef]
69. Williams, C.P. *Explorations in Quantum Computing*; Springer Science and Business Media: New York, NY, USA, 2010.
70. Oliveira, D.S.; Ramos, R.V. Residual entanglement with negativity for pure four-qubit quantum states. *Quantum Inf. Process.* **2010**, *9*, 497. [CrossRef]
71. Sabín, C.; García-Alcaine, G. A classification of entanglement in three-qubit systems. *Eur. Phys. J. D* **2008**, *48*, 435. [CrossRef]
72. von Neumann, J. *Mathematical Foundations of Quantum Mechanics*; Princeton University Press: Princeto, NJ, USA, 1996.
73. Popescu, S.; Rohrlich, D. Thermodynamics and the measure of entanglement. *Phys. Rev. A* **1997**, *56*, R3319. [CrossRef]
74. Bengtsson, I.; Życzkowski, K. *Geometry of Quantum States: An Introduction to Quantum Entanglement*; Cambridge University Press: New York, NY, USA, 2006.